

Systematic Detection of Anomalous Ionospheric Perturbations Above LEOs From GNSS POD Data Including Possible Tsunami Signatures

Heng Yang^{ID}, Manuel Hernández-Pajares^{ID}, Wojciech Jarmołowski^{ID}, Paweł Wielgosz^{ID}, Sharon L. Vadas, Oscar L. Colombo, Enric Monte-Moreno^{ID}, Alberto Garcia-Rigo^{ID}, Victoria Graffigna, Anna Krypiak-Gregorczyk, Beata Milanowska, Pau Bofill-Soliguer, Germán Olivares-Pulido, Qi Liu^{ID}, and Roger Haagmans

Abstract—In this article, we show the capability of a global navigation satellite system (GNSS) precise orbit determination (POD) low Earth orbit (LEO) data to detect anomalous ionospheric disturbances in the spectral range of the signals

Manuscript received February 10, 2022; revised May 26, 2022; accepted June 6, 2022. Date of publication June 13, 2022; date of current version June 23, 2022. This work was supported in part by the COSTO ESA-Funded Project under Grant ESA ITT AO/I-9514/18/NL/IA, in part by the Generalitat de Catalunya Grant 2017 SGR-0851, and in part by the EU Project 101007599—PITHIA-NRF. (Corresponding author: Manuel Hernández-Pajares.)

Heng Yang is with the School of Electronic Information and Engineering, Yangtze Normal University, Chongqing 408100, China, and also with the Research Group of Ionospheric Determination and Navigation based on Satellite and Terrestrial Systems (IonSAT), Department of Mathematics, Universitat Politècnica de Catalunya, 08034 Barcelona, Spain.

Manuel Hernández-Pajares is with the Research Group of Ionospheric Determination and Navigation based on Satellite and Terrestrial Systems (IonSAT), Department of Mathematics, Universitat Politècnica de Catalunya, 08034 Barcelona, Spain, and also with the Institut d'Estudis Espacials de Catalunya—Universitat Politecnica de Catalunya (IEEC-UPC), 08034 Barcelona, Spain. (e-mail: manuel.hernandez@upc.edu).

Wojciech Jarmołowski, Paweł Wielgosz, Anna Krypiak-Gregorczyk, and Beata Milanowska were with the Faculty of Geoengineering, University of Warmia and Mazury in Olsztyn, 10-719 Olsztyn, Poland.

Sharon L. Vadas is with NorthWest Research Associates, Inc., Boulder, CO 80301 USA.

Oscar L. Colombo is with the NASA Goddard Space Flight Center, Greenbelt, MD 20771, USA.

Enric Monte-Moreno is with the Centre for Language and Speech Technologies and Applications (TALP), Department of Signal Theory and Communications, Universitat Politècnica de Catalunya, 08034 Barcelona, Spain.

Alberto Garcia-Rigo is with the Institut d'Estudis Espacials de Catalunya—Universitat Politecnica de Catalunya (IEEC-UPC), 08034 Barcelona, Spain, and also with the Research Group of Ionospheric Determination and Navigation based on Satellite and Terrestrial Systems (IonSAT), Department of Mathematics, Universitat Politècnica de Catalunya, 08034 Barcelona, Spain.

Victoria Graffigna is with the Geodesia Espacial y Aeronomía (GEESA), Universidad Nacional de La Plata (UNLP), B1900 La Plata, Argentina, and also with the Research Group of Ionospheric Determination and Navigation based on Satellite and Terrestrial Systems (IonSAT), Department of Mathematics, Universitat Politècnica de Catalunya, 08034 Barcelona, Spain.

Pau Bofill-Soliguer is with the High Performance Computing Group and Sustainability, Technology and Humanism (CAP-STH), Department of Computers Architecture, Universitat Politècnica de Catalunya, 08034 Barcelona, Spain.

Germán Olivares-Pulido and Qi Liu are with the Research Group of Ionospheric Determination and Navigation based on Satellite and Terrestrial Systems (IonSAT), Department of Mathematics, Universitat Politècnica de Catalunya, 08034 Barcelona, Spain.

Roger Haagmans is with the European Space Research and Technology Centre (ESTEC), European Space Agency, NL-2201 AZ Noordwijk, The Netherlands.

Digital Object Identifier 10.1109/TGRS.2022.3182885

associated with earthquakes and tsunamis, applied to two of these events in Papua New Guinea (PNG) and the Solomon Islands during 2016. This is achieved thanks to the new PIES approach (POD-GNSS LEO Detrended Ionospheric Electron Content Significant Deviations). The significance of such ionospheric signals above the swarm LEOs is confirmed with different types of independent data: *in situ* electron density measurements provided by the Langmuir Probe (LP) onboard swarm LEOs, DORIS, and ground-based GNSS colocated measurements, as it is described in this article. In this way, we conclude the possible detection of the tsunami-related ionospheric gravity wave in PNG 2016 event, consistent with the most-recent theory, which shows that a tsunami (which is localized in space and time) excites a spectrum of gravity waves, some of which have faster horizontal phase speeds than the tsunami. We believe that this work shows as well the feasibility of a future potential monitoring system of ionospheric disturbances, to be made possible by hundreds of CubeSats with POD GNSS receivers among other appropriate sensors, and supported for real-time or near real-time confirmation and characterization by thousands of worldwide existing ground GNSS receivers.

Index Terms—Global navigation satellite system (GNSS), ionospheric indicator of earthquake/tsunami, low Earth orbit satellite.

I. INTRODUCTION

THE coupling of earthquakes and tsunamis with the atmosphere can occur through atmospheric acoustic-gravity waves generated by vertical and horizontal displacements of the ground or sea surface [1]–[5]. Such acoustic-gravity waves propagate upward through the lower atmosphere (up to 50 km, comprising the troposphere and stratosphere) to the upper atmosphere (heights of 50–600 km, including the mesosphere and thermosphere) [6]. Due to the exponential decrease in the particle density with increasing altitude and the conservation of the energy [7], the amplitudes of fast gravity waves (with initially small amplitudes such as occurs with tsunamis) will increase exponentially with altitude until they are dissipated by the exponentially increasing kinematic viscosity in the thermosphere [5], [8], [9]. Until damped by molecular viscosity, these gravity waves induce traveling ionospheric disturbances (TIDs) through neutral-ion collisions. These TIDs are not self-sustaining, though, once a gravity wave is dissipated, it no longer induces a TID.

Through neutral-ion collisions, the ionospheric delay of the carrier phase and pseudorange global navigation satellite sys-

tem (GNSS) measurements gathered by ground and onboard low Earth orbit (LEO) receivers from +100 transmitters orbiting above 19 000-km height is correspondingly affected [10]. In this way, the geometry-free combinations of dual-frequency GNSS carrier phase measurements allow to measure such earthquake- and tsunami-related ionospheric signatures very accurately, typically from the ground (e.g., [11]). The possibility of doing this procedure automatically from available LEO-based GNSS receivers intended for precise orbit determination (POD) is the main challenge studied in this work.

We present two case studies using event-collocated passes of Swarm satellites. The events were the Papua New Guinea (PNG) Mw7.9 and Solomon Islands Mw7.8 earthquakes both occurred in 2016. Swarm satellites carry on both POD GNSS receivers, providing total electron content (TEC) measurements, and a Langmuir-probe measuring the *in situ* electron density (ED), which are useful in order to validate the detection of anomalous TEC perturbations. The validation is completed by analyzing the ground-based GNSS data and DORIS measurements.

Dual-frequency GNSS receivers have become one of the most precise and with widest coverage ionospheric sounding technique in the present times (see, for instance, a reliable GNSS ionospheric monitoring in [12]). In line with the above, Yang *et al.* [11], Artru *et al.* [13], Komjathy *et al.* [14], Occipinti *et al.* [15], and Azeem *et al.* [16] reported the detailed evolution of the ionospheric response to earthquakes and tsunamis, mostly in terms of TIDs, using large-scale networks of ground-based Global Positioning System (GPS) receivers. This wide observational capability of GNSS contrasts with specific and local observations, such as digital Doppler sounders [17], and the OI(${}^3P-{}^1D$) 630.0-nm airglow imagers [4].

The TIDs induced by atmospheric acoustic-gravity waves via neutral-ion collisions can be characterized by ionospheric measurement in the line-of-sight path from the ground-based GNSS receiver to the satellite. The medium-scale TID activities are normally assumed to occur below the maximum height of the F2 layer, where fast gravity waves can propagate, and a sufficient amount of ionized particles interacts with the neutral atmosphere [18]. By assuming this hypothesis, the horizontal behavior of TIDs can be well characterized by ground-based GNSS equipment while neglecting the vertical position and altitude-related characteristics.

LEO satellites, deployed in orbits at altitudes from several hundred to more than 1000 km, provide the opportunity to independently observe the topside ionospheric response to earthquakes and tsunamis by processing POD data from space-borne dual-frequency/multifrequency GNSS receivers with a positive elevation angle. As an illustration, Yang *et al.* [19] and Komjathy *et al.* [20] observed the ionospheric disturbances induced by the 2011 Japan Tohoku earthquake from the GPS POD data of the GRACE LEO satellites above the U.S. Alaska region. Jarmolowski *et al.* [21] and Schmidt *et al.* [22] also reported the topside ionospheric response to 2015 Chile tsunami from the POD data of Swarm and GOCE LEO satellites, which was confirmed by other *in situ* instruments.

In addition, the footprints of earthquakes and tsunamis can also be recorded by alternative measurements taken from LEO satellites, e.g., the seismic signal measured in the middle ionosphere from the range data between two GRACE satellites [23], as well as from the coseismic gravity gradient data of the GOCE satellite [24]. The tsunami-driven gravity waves were also measured by the ionospheric radio occultation (RO) data from COSMIC satellites [25], accelerometer and thruster in the GOCE satellite [26], the Langmuir Probes (LPs) of Swarm satellites [21], and K-/Ka-band interferometer of GRACE satellites [22].

In summary, the use of a large-scale, densely distributed ground-based GNSS observation network has allowed so far a remarkable reconstruction of the detailed characteristics of the near-coast ionospheric footprint of medium- and large-scale earthquakes and tsunamis. This enables a rough estimate of the location and intensity of the earthquake and tsunami [2], [27], [28], and it also makes possible to establish an early earthquake and tsunami monitoring system [11], [29].

With the addition of LEO satellites that could observe tsunami ionospheric features far from land, the use of multisource observations would contribute to increase the effectiveness of the monitoring system [30]. However, it should be noted that there are *a priori* challenges in definitively capturing topside TID activities of earthquakes and tsunamis by onboard POD GNSS observations and other instruments: 1) the LEO satellites should properly cover in space and time the target regions, which will be facilitated by the on-going plans of deploying hundreds of LEOs with onboard GNSS POD receivers and 2) the intensity of the released energy should allow to induce topside ionospheric activity with a detectable intensity. In this regard, and by employing all available observations from the swarm LEO satellites for years, [31] reported a possible connection to earthquakes through *in situ* detected anomalies in ED and magnetic field data.

With the above context in consideration, in this article, we show the potential capability for POD-GNSS receiver measurements from LEO satellites, orbiting at 450 km and above, to detect anomalous ionospheric disturbances (including those associated with earthquakes and tsunamis). This claim is based on two facts.

- 1) A single Chapman model with a linearly increasing height scale describes very well the behavior of the ED above the LEO height (typically above the peak of the F2 layer) [32], [33], which, for instance, allows accurate extrapolation [34], [35]. The smooth behavior at the topside ED allows the measurement of clear signals of an earthquake or tsunami despite the relatively low ionization level and the high elevation at the location of the event.
- 2) The increasing number of CubeSat constellations, which might allow, in the future, a 24/7 applicability of the technique proposed in this work. Currently, there are several hundred CubeSats that can perform ionospheric sounding with GNSS signals. Some companies have deployed CubeSats for RO ionospheric sounding successful [36], [37], despite initial problems due to size and power (e.g., duty cycling impact, see, for instance, [38]).

We propose in this work a methodology that potentially detects earthquake- and tsunami-related signatures in the topside ionosphere, mainly based on the POD data from GNSS receivers onboard LEO satellites: this method is called the PIES approach (POD-GNSS LEO Detrended Ionospheric Electron Content Significant Deviations technique). PIES extends the applicability and scope of our previous multi-technique study of Chile-Illapel 2015 Mw8.3 event [39] to other events. The method includes three steps: the acquisition of significant characteristics, the identification and issuance of warnings, and external validation. This technique might be able to provide potential warnings of earthquakes and tsunamis relying only on GNSS POD observations from future dense constellations of LEO satellites.

We illustrate the application of the PIES methodology to the detection of the possible topside-ionosphere footprints from two earthquakes/tsunamis by using the data of LEO satellites that passed near the respective epicenters at the time of the events.

- 1) On December 17, 2016, an Mw7.9 earthquake and tsunami happened in PNG. We will show how PIES discloses potential earthquake and tsunami ionospheric signatures thanks to the availability of nearby Swarm POD GNSS data. This anomaly is further confirmed by *in situ* Swarm LP ED and ground-based GNSS data.
- 2) In the Solomon Islands 2016 event, an Mw7.8 earthquake and tsunami happened on December 8, 2016, and after applying PIES in a blind way, an important preseismic disturbance was detected. Such ionospheric perturbation has been validated by multiple ionospheric measurements, such as Swarm LP, ground GNSS, and DORIS data. The origin of this perturbation was checked out, but no conventional sources could be found to explain it, including meteorological events. This case study is considered of interest by itself to show the capabilities of PIES as a blind LEO-based anomalous ionospheric perturbation detector.

II. DESCRIPTION OF EXPERIMENTAL DATA

A. Measurements

In this study, the POD data of dual-frequency GPS observations from swarm LEO satellites are used to test the proposed method for detecting the upper anomalous ionospheric perturbations, potentially including those originated from earthquakes and tsunamis. The swarm LEO constellation, composed of three identical quasi-polar orbiting satellites of the European Space Agency (ESA), began to provide 1-Hz GPS observations in middle 2014 [40]. Two of them (Swarms A and C) placed at the orbit of \sim 460-km altitude and the other (Swarm B) at \sim 510 km can record the topside ionospheric activity by GPS POD receivers. The fly design of Swarms A and C, in parallel with a horizontal distance of less than 200 km, facilitates detailed observation of the wavefront motion that can contribute to the analysis of the response of the top ionosphere to atmospheric gravity waves driven by seismic tsunamis.

In addition, other measurements are employed for the validation of the detected data from POD: 1) LP measure-

ment on Swarm satellites for *in situ* ED; 2) GNSS POD measurement from other LEO satellites; 3) GNSS dual-frequency observation of ground network for high-resolution slant TEC (STEC) along the line of sight between GNSS satellites and receivers; 4) DORIS dual-frequency measurement for bottom ionospheric activity (see an example of application in [41]); 5) wind field observation for the background neutral wind activity; and 6) meteorological data and earthquake/tsunami records for confirmation of the potential origin of the ionospheric deviation.

B. Selection of Earthquake/Tsunami Cases

We have found two neighboring regions, PNG and Solomon Islands, where two earthquakes occurred colocated with the passes of Swarm satellites during the studied period, end of 2016. In particular, PNG is located at the connection of four main tectonic plates: Australian, Pacific, Eurasian, and Philippine plates. There are also a number of smaller plates, which makes this region especially active seismically. The time period selected for the analysis covers November and December 2016. November is relatively seismologically quiet and includes two weeks, during which no earthquake of magnitude equal to or above 5.0 occurred. The threshold of 5.0 for the selection of earthquakes in this work is assumed approximately, by inferring from the existing works on the sensitivity of ground GNSS data to the seismic activity (see [42] and [43]), as well as from recent works on the sensitivity of Swarm magnetic data to earthquakes of similar magnitude [44]. December 2016 was very active seismologically with two earthquake events having magnitudes of 7.8 and 7.9, both triggering tsunamis. There were almost 150 earthquakes equal to or above the magnitude of 5.0 from the beginning of November 2016 to the end of December 2016, most of which were aftershocks and took place after December 8, 2016. The orbits of Swarm satellites, which have an inclination around 87.35° , pass the edge of two subducting tectonic plates (Australian and Pacific) at a quite large angle.

III. TECHNIQUES FOR DETECTION AND VALIDATION

In this section, the techniques for detecting and recognizing significant topside ionospheric disturbances in the spectral range of the earthquake and tsunami ionospheric footprints from GNSS POD data will be described in detail. The approaches used for validation have been the evolutionary power spectrum technique for analyzing ED from LP measurement, as well as the simple detrending technique for analyzing other measurements, such as DORIS and ground GNSS observations.

A. PIES: POD-GNSS LEO Detrended Ionospheric Electron Content Significant Deviations

One challenge in the sounding of the ionosphere by GNSS POD data, and by any other onboard instrument, such as the LP measuring *in situ* ED, is that the LEO satellites move at high-speed (e.g., around 7.5 km/s for the Swarm satellites). This fact makes it difficult to determine the local response of the ionosphere to a given event, which requires the LEO

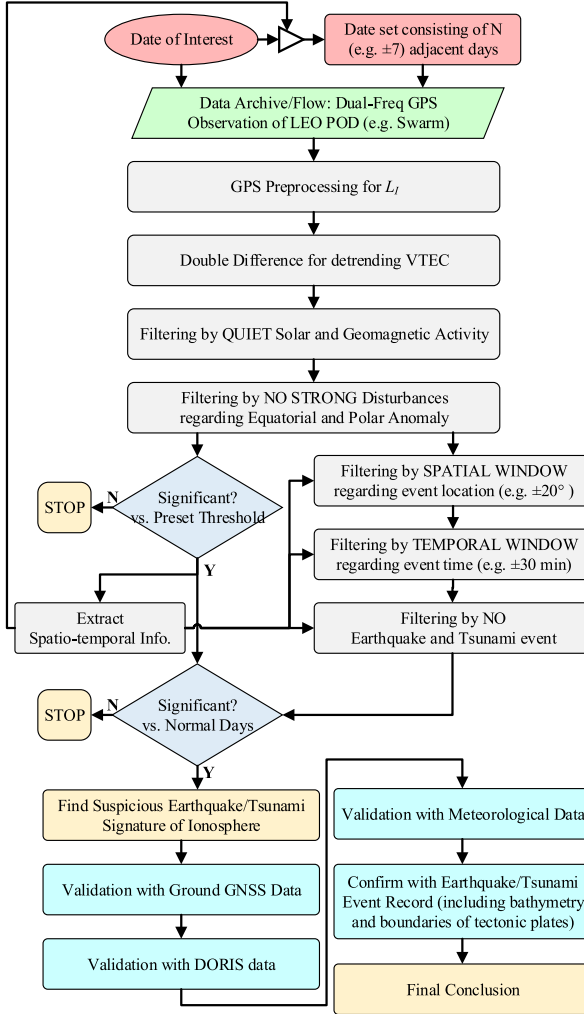


Fig. 1. Flowchart of PIES.

satellite to pass close to the region at the time of the event, i.e., at a distance of less than several hundreds of kilometers from the epicenter. This is the typical distance between the representative points of the ionospheric measurements of different GNSS transmitters observed from a given LEO POD GNSS receiver,¹ which allows some of them to be located very close to the epicenter. Fortunately, the availability of more LEO satellites can definitely provide enhanced ionospheric sounding.

For each given region of interest, PIES requires the time series of detrended ionospheric electron content from GNSS POD data, finds out the significant disturbances by excluding the signatures of known origins and comparing with adjacent (previous, in real-time functioning) normal days, and, finally, validates the disturbance detection from other measurements. The PIES approach comprises two principal phases summarized in Sections III-A1 and III-A2, and each of them includes different steps (see Fig. 1).

1) *PIES First Step: Ionospheric Wave Signature Retrieval From GNSS POD Data:* The orbital speed of the LEOs, v_{LEO}

(7.5 km/s for the Swarm satellites), is way higher than the highest horizontal velocities v_{TID} of the possible ionospheric signals to be detected by the LEO (e.g., from few hundreds of m/s for gravity waves [13] to 1 km/s around 450-km height for the acoustic waves following [45, Fig. 1]). Therefore, the sounding from the LEO is considered as a snapshot of any crossing ionospheric wave. In this way, we can easily estimate the ionospheric wave $\lambda_{\text{TID}} \approx v_{\text{LEO}} \cdot T_{\text{TID@LEO}}$ from the observed periods $T_{\text{TID@LEO}}$ with the highest energy. Then, we can calculate the approximate actual period $T_{\text{TID}} \approx \lambda_{\text{TID}}/v_{\text{TID}}$ from the estimated TID horizontal velocity v_{TID} (see points 3 and 4 at next—second—PIES step), taking into account as well the relative movement LEO—ionospheric wave. This is important in order to determine whether the actual wave period is above or below the buoyancy period, around 5–8 min [46], i.e., to figure out whether we are detecting a gravity or an acoustic wave. Another aspect to double-check what kind of wave we are sensing is to estimate the vertical velocity, which should be at least 300 m/s for an acoustic wave, being likely a gravity wave for lower values.

The main observation in PIES is the ionospheric combination (also called geometry-free combination) $L_1 = L_1 - L_2$ of the carrier phase measurements L_1 and L_2 in both GPS POD receiver frequencies and expressed in length units. As it is well known, L_1 mainly depends linearly on the along line-of-sight integrated ionospheric ED, i.e., STEC or (S), and on the carrier phase ambiguity $B_1 = B_1 - B_2$, which can be considered constant for each phase-continuous transmitter-receiver arc, and then completely removed after a simple detrending (see the review paper [10] for details after a general introduction on *GNSS Ionosphere*).

S mainly contains typical trends of TEC, such as diurnal variations and elevation angle variation, which are characterized by extremely low frequencies and very high energies. It also contains ionospheric perturbations with lower energies at higher frequencies, such as Medium Scale TIDs (MSTIDs, see, for example, [47]), including the circular wave signature of earthquakes and tsunamis [11].

Instead of the typical usage of bandpass filters to separate the disturbance components, PIES uses an alternative efficient solution directly based on the double time difference of the measured ionospheric combination of carrier phases, L_1 . The detrended STEC can be directly obtained as $\tilde{S} \approx L_1(t) - (1/2)(L_1(t - \tau) + L_1(t + \tau)) = (-1/2)\delta^2 L_1$. In this way, the phase bias of L_1 , constant in continuous phase arcs (i.e., in between cycle slips), cancels out. Furthermore, the energy of trend components decreases, and at the same time, the terms with periods T around twice the time interval τ considered in the double time difference are amplified (see details in [18]).

Moreover, the motion of the ionospheric observing points is taken into account in PIES. It is especially significant in our scenario of LEO-based measurements where the GNSS receivers are moving at very high speed, up to more than one order of magnitude higher than the ionospheric waves. The corresponding effect in the expected periods² can be

¹Known as *ionospheric pierce points* (IPPs) in the GNSS community.

²The Doppler effect.

considered in a simple way in PIES: assuming, as it has been commented above, that the ionospheric waves appear almost “frozen” in front of the fast movement of the sensors (like the GNSS POD receiver and LP) onboard the LEO. Considering as well different orientations between the LEO and the ionospheric wave velocities, the range of potential periods of earthquake- and tsunami-related ionospheric TIDs measured from swarm LEOs goes approximately from 10 to 240 s.

The selection of the optimal time difference $\hat{\tau}$ to perform the double time difference detrending allows revealing the ionospheric response to the tsunami.

In PIES, the mapping function M approximation is applied. In other words, it is considered that the modeled detrended vertical TEC (VTEC, defined as \tilde{V}), which can be derived from the LEO STEC ($\tilde{S} = \tilde{V} \cdot M$) (see [10]) is located on a spherical thin-shell layer placed at a mean effective height. Such approximation works better at high than low elevation angles. Therefore, in order to reduce the ionospheric mismodeling, the mapping function hypothesis may yield, and the observations with an elevation angle of less than 40° are discarded.

2) PIES Second Step: Warning of Potential Anomalous Ionospheric Signature: A warning of potential anomalous ionospheric disturbance will be issued by PIES once a sudden increase appears in the temporal evolution of the power of the detrended VTEC \tilde{V} on the passes of the LEO satellite. Such an increase is estimated by comparison with the previous \tilde{V} values measured in the same region and at similar times. In this way, the seasonal ionospheric signatures like those of seasonal MSTIDs are not taken into account implicitly. In order for the PIES to declare an ionospheric disturbance as potentially significant, the following evidence must be met.

1) *Comparison With a Record of Adjacent Normal Days:*

Note that some of the disturbances of different origins are difficult to distinguish from the tsunami-driven ones. This is due to them having quite similar features in terms of time and frequency (see, for instance, MSTID climatology in [11] and [47]). The adopted solution in PIES is to compare the disturbances with the record of previous $2 \cdot n$ days in real time or $\pm n$ days in postprocessing (e.g., with $n = 8$ or $n = 13$) by means of an identical spatial window (e.g., $\pm 20^\circ$ w.r.t. the location of the event), time of day window ($\pm 30\text{--}90$ min w.r.t. the time of the event), and the normal day window that filters out the days with strong activity due to either space weather or any earthquake/tsunami events.

2) *Discard Disturbances Regarding Space Weather or Equatorial/Polar Anomalies:* It is possible that the detected ionospheric waves are induced by unusual conditions of space weather, such as the strong solar activity or geomagnetic activity. Alternatively, there could be ionospheric anomalies as the LEO satellites pass over equatorial and polar regions. Therefore, those components of the disturbances, corresponding to expected equatorial and polar region ionospheric anomalies, will be dropped.

3) *Estimation of Propagation Parameters in Time and Space:* The determination of the propagation parameters should be done ideally in real time when possible, or at

least in near real time, by means of rapid and efficient determination models or algorithms, such as, for example:

- a) the rough parameter inspection from time and frequency analysis for the POD GNSS observation of a single LEO satellite compared with velocity estimations from keograms based on MSTID-detrended L_1 from ground-based GNSS receivers;
 - b) the technique of direct GNSS Ionospheric Interferometry (see [48]) for the case when tandem LEO satellites (such as in Swarm case) are available;
 - c) alternatively, the atomic decomposition detector of the MSTIDs’ technique provides as well velocity estimation, when a minimum density and the number of permanent ground-based GNSS receivers are available [11], [49].
- 4) *Confirm Spatiotemporal Propagation Consistency With Earthquake/Tsunami Source:* The estimated propagation parameters allow for the exclusion of components of ionospheric signature that has low relevance compared with the earthquake and/or tsunami contribution. Thus, the ionospheric signature would be excluded or marked as “low confidence.” The spatiotemporal information related to the disturbances that are compatible with the propagation of the tsunami is retrieved and compared with additional information for double checking the feasibility of the earthquake/tsunami signature detection. An example is the consistency of the velocity evolution of the detected TID signal compared with the sea floor depth changes. The above considerations are used, for instance, to declare or not the PIES warning of a potential tsunami.

B. Short-Term Fourier Transform and Time-Varying Electron Density Power Spectra

The discrete Fourier transform (DFT) decomposes discrete signals in sinusoidal components that model the features that are useful for the additional validation of the potential earthquake or tsunami ionospheric footprint detection, beyond the simple PIES detrending procedure previously introduced. The signal of the time samples function $x(t)$ can be decomposed into frequency components $X(\omega)$ covering the entire ω discrete frequency range. This frequency-domain representation can be also transformed back exactly to $x(t)$ by the inverse DFT. The square of the absolute value of the DFT values in the frequency domain provides the spectral power density at individual frequencies.

An efficient method of signal analysis in time is short-time Fourier transform (STFT), which is timewise, sliding window of DFT applied sequentially on the input signal. This sliding window procedure allows for tracking the change of position of the spectral peaks. The STFT plots allow to characterize the sequential time changes of the signal in the frequency domain. The evolutionary and windowed power spectrum is a modification of the DFT method, which computes the spectrum of overlapping segments of the time series. The evolutionary power spectrum can be calculated by the STFT. The output of STFT is the short-term, time-localized frequency power of the signal. The data sequence to be transformed is

multiplied by a window function, which is nonzero for only a short period of time [50]. The STFT of the signal is computed as the window is sliding along the time axis, resulting in a 2-D representation of the signal. Mathematically, this is expressed as

$$\text{STFT}_{f,t} = \sum_{n=0}^{N-1} x_n w_{n-t} W_N^{fn}, \quad f = 1, 2, \dots, N-1 \quad (1)$$

where x_n is a sequence of discretized time-domain signal to be transformed, f is the harmonic number, n is the number of sample, N is the number of all samples, $W_N = e^{(i2\pi/N)}$, w_n is a sequence of a discretized window function, and t is its time sample index. The applied window is the Tukey window. The Tukey window, also known as the cosine-tapered window, can be regarded as a cosine lobe of width $(r/2)(N-1)$ that is convolved with a rectangular window of width $(1-(r/2))(N-1)$. The function of the window is to reduce the variability associated with the Periodogram. The equations defining Tukey window $w_{TU}(n)$ are

$$\begin{cases} \frac{1}{2} \left[1 + \cos \left(\frac{2\pi}{r} \frac{n-1}{N-1} - \pi \right) \right], & n < \frac{r}{2}(N-1) + 1 \\ \frac{1}{2} \left[1 + \cos \left(\frac{2\pi}{r} - \frac{2\pi}{r} \frac{n-1}{N-1} - \pi \right) \right], & N - \frac{r}{2}(N-1) < n \\ 1, & \text{otherwise} \end{cases} \quad (2)$$

where r is the ratio of taper to constant sections and is between 0 and 1.

For a fixed time, STFT of a data sequence x_n describes its local frequency content near the sample at moment t as a function of the discrete frequency f . These frequency representations form, then, the image or a 3-D surface, the shape of which depends on the window size and overlap size. This essentially corresponds to the computation of the STFT squared magnitude of the signal sequence x_n , that is, for a window width n , as follows:

$$\text{SP}_{f,t} = |\text{STFT}_{f,t}|^2. \quad (3)$$

C. Other Validation Approaches for PIES Warning

Once a potential warning of earthquake-/tsunami-driven disturbances by PIES is issued, the warning validation should be done in the next stage. This validation can be based on different ionospheric observation approaches:

- 1) *Validation With Ground GNSS Data and Other LEO GNSS Data:* The ground GNSS data, in the PIES approach, provide a reliable way of confirming the potential tsunami-/earthquake-related ionospheric warnings provided by Swarm based on its heritage in the TID modeling (see for instance [47] and [48]) and the recent improvements, especially with dense and large networks with a positive impact on its application for studying composed phenomena [11], [49], [51].
- 2) *Validation With DORIS Data:* DORIS dual-frequency measurements, at 2036.25 (S1) and 401.25 MHz (U2), from the 51 ground transmitters to the five available

LEO PODs onboard, such as Cryosat-2 (CS2), JASON-3 (JA3), HY-2A (H2A), Sentinel-3 (S3A), and Saral (SRL) flying at different LEO heights, have been also considered in this study. They contribute to the validation of the results under PIES obtained associated with PNG and Solomon Islands earthquakes and tsunamis, providing detrended TEC measurements below the DORIS transmitters onboard such LEOs.

- 3) *Validation with the multi-GNSS and multisystem ionospheric tomography, including DORIS data as well* [41].
- 4) *Validation With Meteorological Data:* The background wind data on a neutral atmosphere will be investigated as well. This can allow the discarding of a strong wind event in the lower to the middle atmosphere that might influence the AGW propagation [52] and create potential tertiary gravity waves that originate from the dissipation of mountain waves [53], [54]. Strong rainfall events can be checked as well, following recent results in [55]), looking for instance in [56].
- 5) *Confirmation With Earthquake/Tsunami Event Record:* Investigate the occurring location and time of disturbance if it shows the coherent characteristics with a tsunami, e.g., the velocity of disturbances similar to the tsunami along with bathymetry and boundaries of tectonic plates.
- 6) Comparison with hydrodynamic models of the ocean to predict the size, shape, and likely path of tsunami disturbances to help confirm or correct the hydro model results using the satellite ionospheric footprint derived results [57] and vice versa.

The final PIES warning is released once the disturbances are confirmed by other approaches of ionospheric sounding.

IV. 2016 PAPUA NEW GUINEA EVENT: ANOMALOUS IONOSPHERE SIGNATURE FROM SWARM POD

On December 17, 2016, a tsunami event occurred in PNG, giving rise to a maximum height of 1 m, which was triggered by a 7.9 magnitude earthquake that occurred at 10:51:12 UTC.

We selected this first event because the Swarm satellites A and C passed few hundreds of kilometers east of the epicenter, about 45 min after the main earthquake shock. The trajectories of the representative points of the ionospheric GNSS POD receiver observations (in cyan points) versus the epicenter (in red star) are shown in Fig. 2. We took a proxy value of 900-km height for computing them, which is suitable under the adopted elevation mask of 40° and the associated small ionospheric mapping function error affecting the VTEC estimation. Then, we had the chance to see if the corresponding POD GPS observations might contain an anomalous ionospheric footprint.

A. Inspection of PIES Warning

As the first step to apply the PIES technique introduced in Section III-A, the ionospheric signatures with time steps of $\{\tau = 2^k : k = 0, \dots, 8\}$ s = $\{1, 2, 4, 8, 16, 32, 64, 128, 264\}$ s are searched from the corresponding double time difference

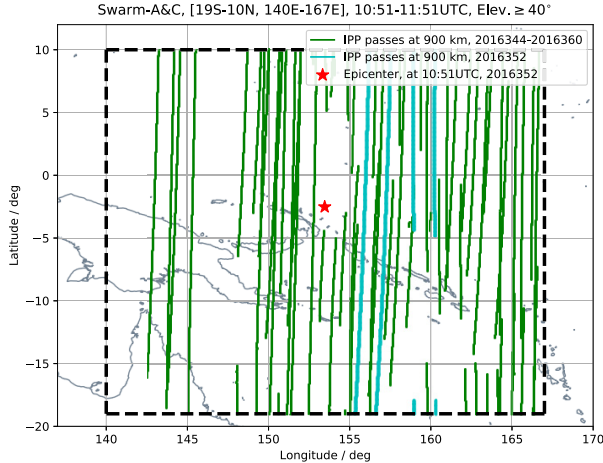


Fig. 2. Location of the ionospheric observations (in cyan) of Swarms A and C regarding GPS satellites within 1 h after the main shock of the 2016 PNG earthquake, at few hundreds of kilometers east from the epicenter, with a spatial window (140°E – 167°E versus 19°S – 10°N), with an elevation mask of 40° . The green lines correspond to the 16 adjacent normal days, with the same spatiotemporal window, and elevation mask as the earthquake day, and the red star for the epicenter.

detrending of the three Swarm GPS POD receivers (Swarms A, B, and C), and they are compared with the values at the same region up to one week before and after (in real-time mode up to few weeks before). Taking into account the expected range of ionospheric wave periods discussed in Section III-A1, the initialization of the double difference (i.e., the bandpass filter) would be done by looking for the optimal time step. The resulting detrended values (see Fig. 3) clearly show one period, associated, in particular, with a time difference of $\tau = 8$ s (i.e., a maximum relative energy at a period of $T = 16$ s), where the energy is the larger one during the whole period analyzed of 17 days of Swarm passes. This is compatible with the expected apparent periods previously discussed and was confirmed by examining the maximum ratio of the energy of the disturbances within 1 h during the main shock with respect to the energy within the same spatial window during 16 adjacent days (see again Fig. 3). Note that the other distinct disturbances in Fig. 3(d), such as those on days 344, 353, 354, and 356 in 2016, contain significant low-frequency components, as confirmed by the double-differential bandpass filtering results with different time intervals [see the results in Fig. 3(g)–(i)]. Compared to the PNG earthquake/tsunami of interest, these disturbances exhibiting different types of characteristics may be driven by different sources that are seen as data noise in this work.

Note that a spatial window of 140°E – 167°E versus 19°S – 10°N is employed for looking for significant detrended VTEC values. The target time interval is about 10:00–12:00 UTC (i.e., 20:20–22:20 in the local night) when the equatorial effect of the ionosphere would not be significant. The geomagnetic equatorial index $Dst = 3$ nT [58], the planetary 3-h-range index $Kp = 3$ [59], and the GOES X-ray flux measurement of Class-A [60] all indicate quiet space weather conditions, with no significant disturbances originated by the phenomena such as major solar activity, solar flare, or geomagnetic storm disturbances.

The detrended VTEC was computed by the double time difference with the optimal time step of 8 s. This showed the significant disturbances about 45 min after the earthquake/tsunami. The possible confounders were also tested, and their presence was ruled out. The disturbances located several hundreds of kilometers from the epicenter exhibit a signature compatible with the response to the tsunami both horizontally in time and space. Since tsunami-driven disturbances display propagation parameters similar to those of MSTIDs, in PIES applications, we have used the ionospheric state on 16 adjacent normal days, as a reference for discarding that the disturbances detected are seasonal features of ionospheric disturbances. Note that, for this event, these normal days are not affected by strong space weather records; see the location of the ionospheric observations in green in Fig. 2. Fig. 4 shows that the zoomed-in view of the results presents the most significant detrended VTEC during 1 h after the main shock.

The much stronger power of the disturbances on the earthquake day compared to that on the normal days might indicate the ionospheric response to the earthquake/tsunami. Two GPS receivers onboard Swarms A and C provided the observations right after the main shock (Mw 7.9), sensing at an elevation angle above the LEO horizon ($\geq 40^{\circ}$). Regarding GPS satellite PRN 32, the line-of-sights that crossed the full main shock target region from the north to south show the maximum power of the disturbances. Fig. 5(a) shows the detrended VTEC regarding GPS satellite PRN 32 and Swarms A and C. Most pronounced VTEC oscillations reach Swarm A before Swarm C, i.e., in order of the 3-D distance to epicenter [see Fig. 5(b)].

Considering the tsunami wave distribution in space and time, this signal might have an associated frequency compatible with the expected one for tsunamis and detected around 45 min after the earthquake. It might also be related to the tsunami due to its appearance at this time and distance from the epicenter but also in this region located in the south of the chain of islands. The furthermost distant satellite (Swarm C) appears as the most affected, especially at the south of the chain of islands: it might be that Swarm C reached “on-time” the region where the tsunami induced some ionospheric disturbance signals, whereas Swarm A would have been “late,” except for the biggest signal, which would correspond to different waves (otherwise, the travel time between them would be too short, ~ 20 s for ~ 100 km). In any case, the signals, not aligned regarding the epicenter, might correspond to different wavefronts, which would be consistent with the circular ionospheric acoustic-gravity waves reported in [11].

Once the main target of the new PIES technique is fulfilled (i.e., detection and warning on anomalous ionospheric wave signatures), we proceed to estimate the type of ionospheric wave. This is done by estimating the ionospheric wavelength first and then the actual period. In addition, the vertical velocity is also estimated for such a goal.

Following the above introduced notation, the horizontal wavelength of the TID, λ , can be estimated as $\lambda \simeq v_{\text{LEO}} \cdot \cos \beta \cdot T_{\text{TID@LEO}} \simeq 130$ – 260 km. Assuming that the wavefront propagates with spherical symmetry, β is the angle between

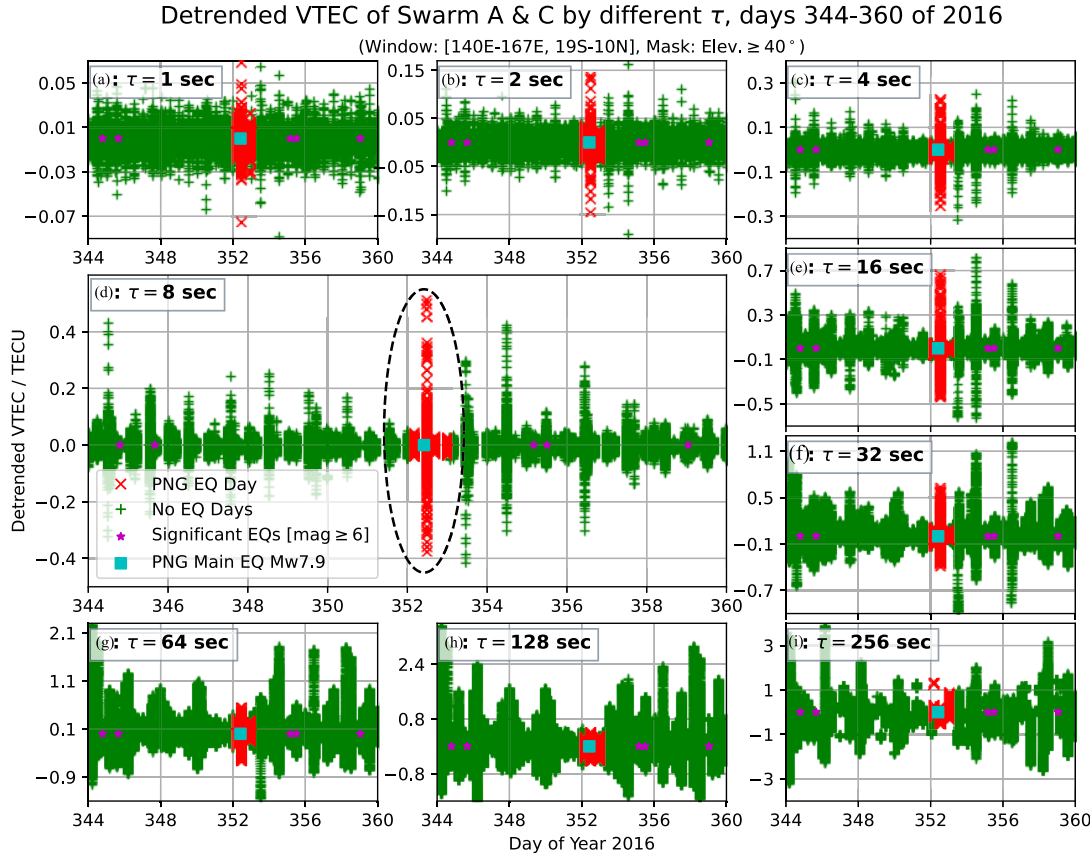


Fig. 3. PIES detrended VTEC computed from Swarms A and C POD GPS data with an elevation mask of 40° is represented versus time during 17 days (in green) around the PNG earthquake, happened on 10 h and 51 min of day 352 of 2016 (with values marked in red), and for a spatial window (140°E – 167°E versus 19°S – 10°N) around the epicenter. This is represented for different detrending time steps $\tau = 1, 2, 4, 8, 16, 32, 64, 128$, and 256 s in (a)–(i). The common legends can be seen in plot (d), in large size to emphasize that the larger detrended VTEC value happens very close to the earthquake main shock, and for $\tau = 8$ s consistently with the expected values considering the high movement of the LEO and the expected wavelengths of the ionospheric waves. The blue star is for the location of the significant earthquakes ($\geq \text{Mw } 6$).

the LEO velocity and the wavefront propagation directions. For the location of the highest detected detrended peak in Fig. 5(b), $\beta \simeq 30^\circ$. The dominant period components $T_{\text{TID@LEO}} \simeq 20\text{--}40$ s can be directly observed from spectrograms of the detrended VTEC of Swarms A and C (see Figs. 11 and 13) at $\sim 11:35$ UTC when the disturbances are of highest intensity. Note that a different but much weaker component $T_{\text{TID@LEO}} \simeq 30\text{--}40$ s is shown between 11:32 and 11:34 UTC, particularly indicated in Fig. 13. As an independent measurement for TIDs by means of Swarm spaceborne LP, the spectrograms of ED disturbances shown in Figs. 10 and 12 confirm the spatial evolution of the period components. A rough estimation of the actual TID period at $\sim 11:35$ UTC yields $T_{\text{TID}} \simeq (\lambda/v_{\text{TID}}) \simeq 217\text{--}433$ s, where the horizontal TID velocity $v_{\text{TID}} \simeq 600$ m/s is estimated correspondingly from the keogram [see Fig. 7(b)], taking into account the horizontal distance of the epicenter-LEO pass with the disturbed signal and the elapsed time from the main shock to the corresponding detection time. The approximation for the TID period during 11:32–11:34 UTC is $T_{\text{TID}} \simeq (\lambda/v_{\text{TID}}) \simeq 500\text{--}650$ s with the corresponding horizontal TID velocity of $v_{\text{TID}} \simeq 400$ m/s. Since the period variation of TIDs along Swarm IPP passes is associated with

the horizontal distance from the epicenter, it may indicate that the proposed ionospheric disturbances have at least one more origin, such as the EQ-driven acoustic waves and the tsunami-driven gravity waves.

This estimation of $v_{\text{TID}} \simeq 400$ m/s at 11:32–11:34 UTC is a bit larger than the horizontal velocity component of the main gravity wave excited by the tsunami as it is the case (see [13, Fig. 1] and associated comments). However, these references assumed that a monochromatic gravity wave is continuously excited by a tsunami as it moves across the ocean, and this gravity wave has the same horizontal phase speed as the tsunami. In fact, the simulated tsunami maximum amplitude, travel times, and the ocean depth shown in Fig. 6 indicate that the tsunami is localized in space and time; therefore, an entire spectrum of gravity waves is excited [5]. This includes gravity waves traveling with a similar horizontal phase speed as the tsunami, as well as gravity waves that have much faster horizontal phase speeds [5]. These latter gravity waves reach the thermosphere faster and are less prone to dissipation from molecular viscosity; therefore, they are quite important in the F region. Note that Makela *et al.* [4] observed gravity waves that had much faster horizontal phase speeds than the tsunami, thereby supporting this work.

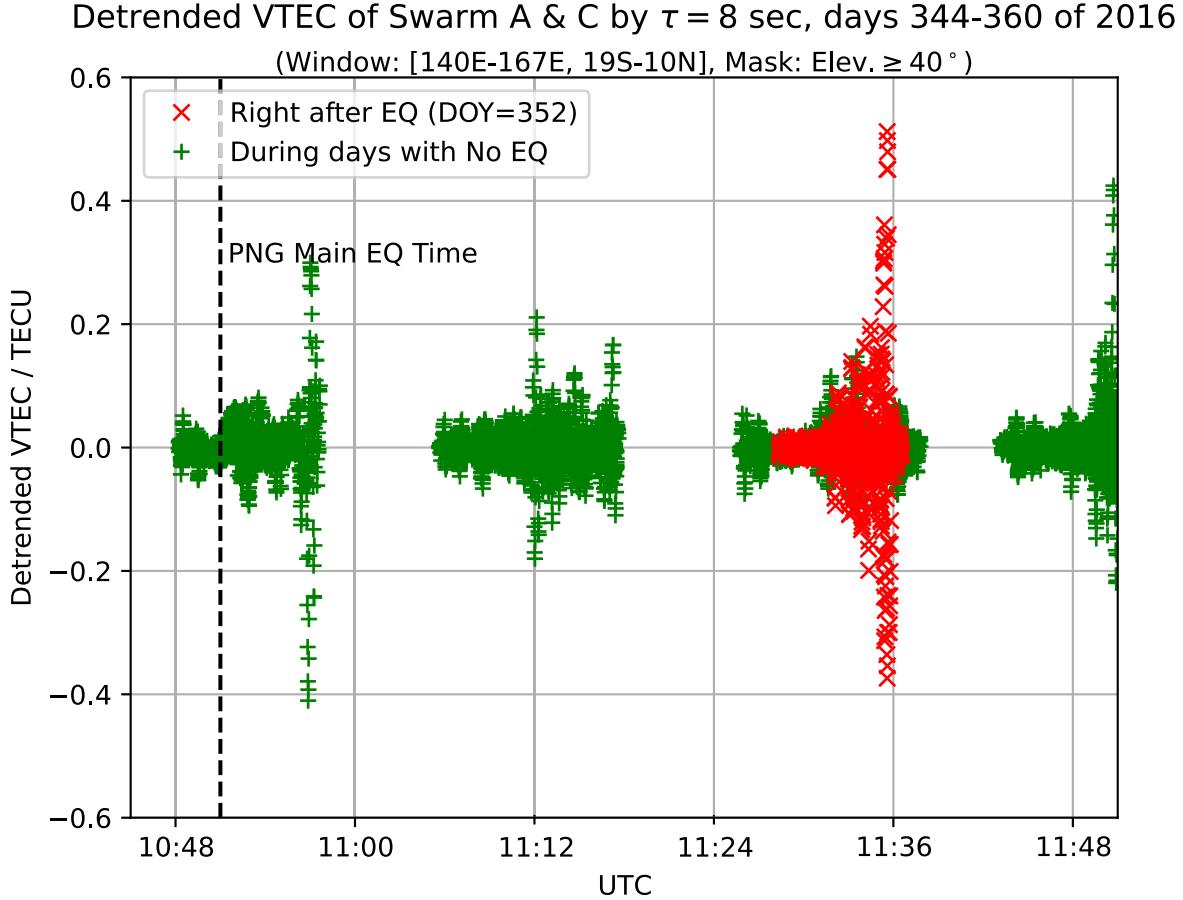


Fig. 4. Time evolution of detrended VTEC for the Swarms A and C POD GPS data already shown in Fig. 3 (PNG earthquake, 10:51 UTC of day 352, 2016) but during 1 h after the main shock (in red scatters), compared with 16 normal days with no earthquake record (in green scatters), with $\tau = 8$ s. For the settings of spatial window and the elevation mask, see Fig. 3.

Moreover, the guess of observed period $T_{\text{TID}} \simeq 217\text{--}433$ s at $\sim 11:35$ UTC is similar to the abovementioned value of the buoyancy period (around 5–8 min), which indicates the option of an acoustic wave associated with the earthquake main shock. Moreover, the much greater period $T_{\text{TID}} \simeq 500\text{--}650$ s during 11:32–11:34 UTC shows the potential detection of the gravity wave originated at the tsunami event.

In order to double-check the possible tsunami origin of the measured perturbation, we consider now the vertical velocity, which should not be larger than 50 m/s for a normal monochromatic wave assumption [13]. For a more realistic model, however, the vertical phase speed can be up to 300 m/s [5, Figs. 10(f) and 16(f)]. The mean vertical velocity found is also compatible with the hypothesis of the tsunami origin: indeed, to reach the Swarm orbital height of 460 km with the delay shown by the largest signal after the main shock (around 45 min = 2700 s), a vertical velocity of 460 km/2700 s = 170 m/s would be needed, which agrees with the model of [5], similar to [4], and significantly smaller than the vertical velocity of the acoustic waves, greater than 300 m/s.

B. Validation of Swarms A and C Langmuir Probe ED and Topside TEC Data by Power Spectra Analysis

In this section, the STFT analysis of ED directly measured by Swarm A and Swarm C LPs (product from Electric Field

Instrument, EFIXLP) and corresponding topside STEC from Swarm A and Swarm C (product TEC_TMS_2F) are used for independently confirming the PIES tsunami warning signal due to the detected ionospheric disturbances. This validation is supported by spectrograms of evolutionary power spectrum density (PSD), and its second purpose is to compare disturbed *in situ* ED signal and topside TEC signal disturbed from the same seismic events. It should be pointed out that these two kinds of signals refer to geometrically different spatial locations, and therefore, an approximate similarity could be expected, rather than absolute coherency of the signals.

The analysis of Swarms A and C *in situ* ED and topside TEC to selected GPS satellites are based on high-pass filtered data. The DFT has been applied for this purpose, and the cutoff period was heuristically set up to 50 s, which stems from the considerations about the sizes of seismically driven ionospheric disturbances in Section IV-A. All the data were high-pass filtered by removal of the signals with periods longer than 50 s, and then, the spectral analysis by STFT was applied. The spectrograms were then sampled at a 40-s period for plotting together with GIMs in left subfigures adjoined to all spectrograms in this work. These PSD samples show their magnitudes and locations of Swarm disturbances occurring during the analyzed times. The spectrograms were calculated

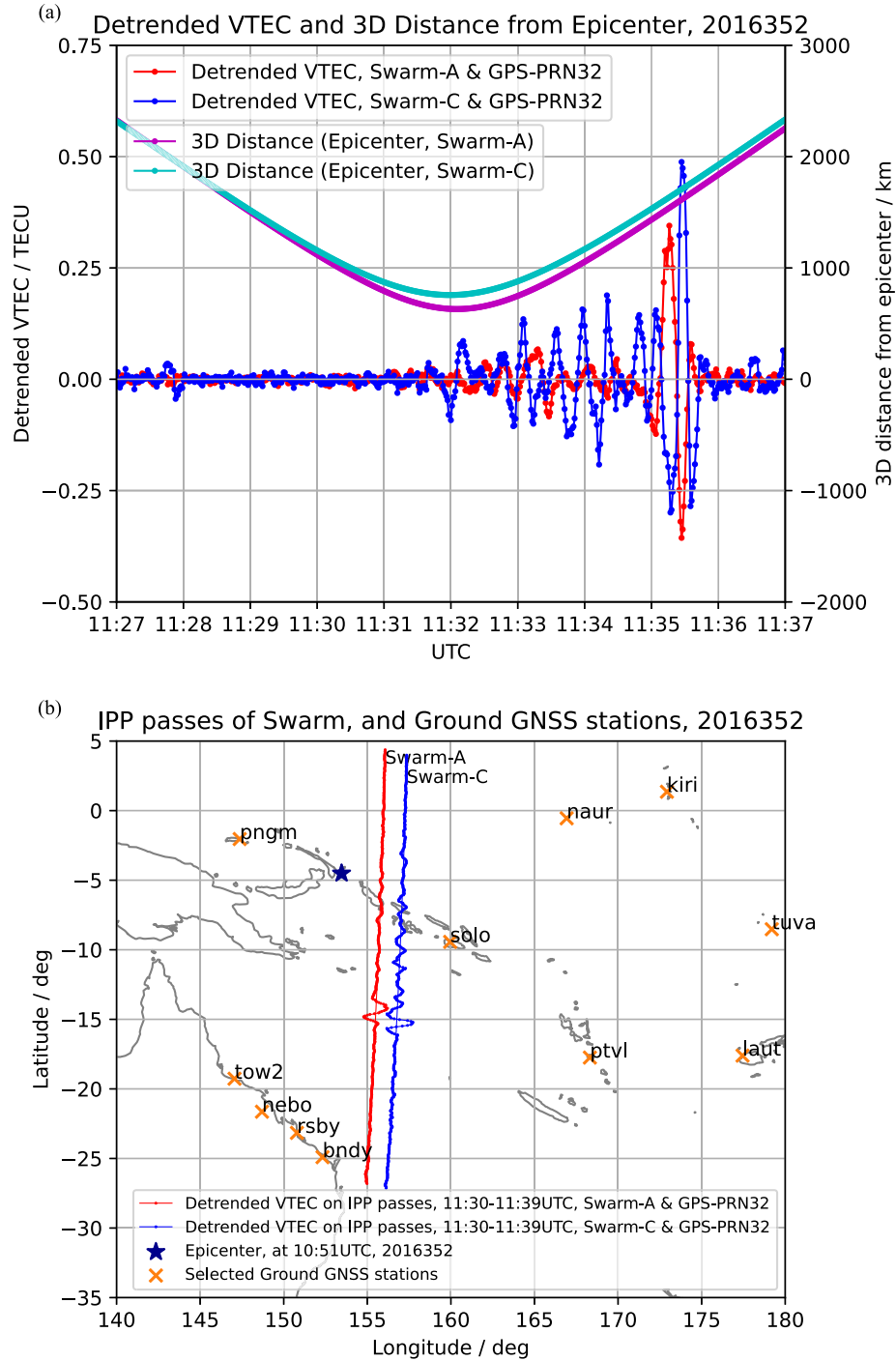


Fig. 5. (a) Evolution versus time (x-axis) of the 3-D distance of GPS PRN 32 satellite ionospheric observation points to the epicenter of PNG earthquake (10 h and 51 min of day 352, 2016) in thousands of km (magenta and light blue lines) and the detrended VTEC in total electron content units (TECU, 1 TECU = 10^{16} m^{-2}), red and green lines, about 1 h after the main shock for Swarms A and C, respectively, with the settings of spatial window and elevation mask of Fig. 3. (b) Spatial evolution of detrended VTEC horizontally overlapping the trajectories of the observing points regarding the GPS satellite PRN 32 and Swarms A (red) and C (blue), with the epicenter marked in blue star. Nearby selected ground GNSS receivers are also represented on the map.

with the use of STFT and windowing using the Tukey window with its main parameter $r = 0.4$ [see (2)]. The width of the window was set to 220 s, whereas the frequency range of spectra is from 90 to 10 s. The scales of the spectrograms and their samples at the selected period are the same for all figures referring to the same quantity, i.e., ED or TEC.

The subjects of validation are Swarm A and Swarm C corresponding trajectories, i.e., close in time and space, and recorded on December 17, 2016, around 11:30 UTC, which is ~ 40 min after the largest EQ ($M_w = 7.9$) occurred close to the eastern coast of New Ireland island (10:51 UTC). Figs. 8 and 9 describe additional trajectories for the previous

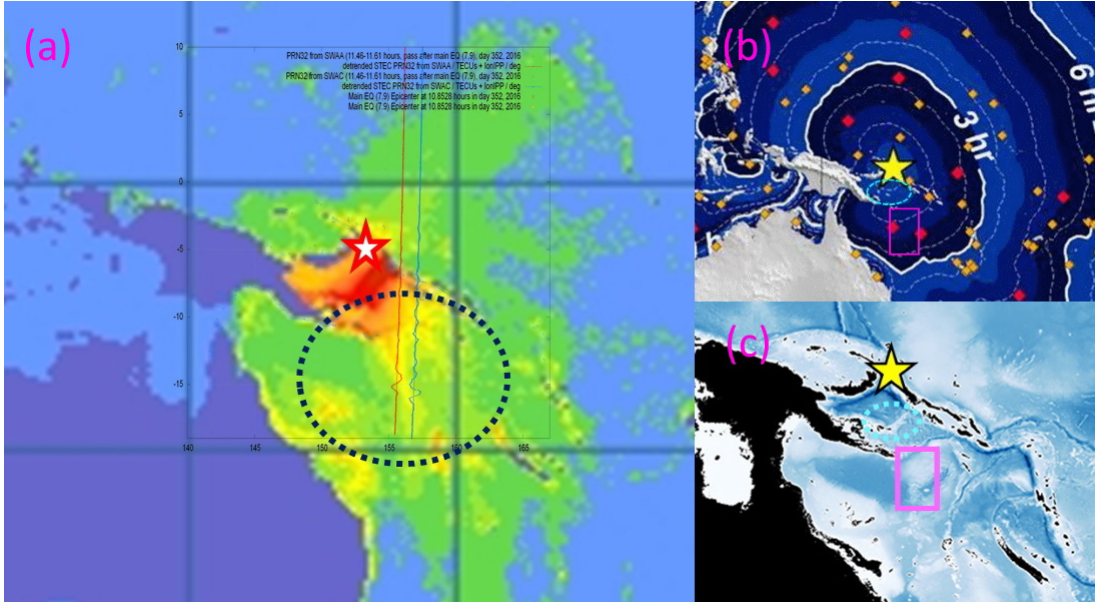


Fig. 6. (a) Detrended VTEC overlapped on the trajectory of the ionospheric observing points regarding GPS satellite PRN 32 Swarms A and C, attached with the tsunami maximum amplitude graph, ranging from 0 (blue) to 100 cm (red), with intermediate growing values in green, yellow, and orange (source from [61]). (b) Zoomed tsunami travel times, source from [61]. (c) Zoomed ocean depth, white for the shallow part and blue for the deep sea (up to -8000 m in black), originating from the earth observatory of the U.S. NASA blue marble with topography and bathymetry, the yellow star for the epicenter, magenta rectangular for ionospheric observing points with higher detrended VTEC, and the cyan ellipse for the tsunami with the highest wave.

to EQ day, at similar time of the day. This reveals significantly smaller disturbances in ED with respect to December 17. It is easily noticeable that, even if Fig. 9 shows a bit larger disturbance for Swarm C ED than Fig. 8 for Swarm A ED, Figs. 10 and 12 illustrate significantly larger perturbations after the mainshock, which confirms the meaning of major EQ having Mw = 7.9.

Fig. 10 shows ED spectrogram for Swarm A on December 17 at around 11:30 UTC, which is ~ 40 min after Mw = 7.9 EQ. Fig. 11 corresponds to Fig. 10 although it shows the topside TEC from dual-frequency GNSS receiver for the selected satellite. It should be pointed out that the GPS satellite was here selected because not all geometrical directions to GPS satellites can find disturbing signals similar to that in ED from LPs. This comparison was also suspected to show only an approximate similarity of signal PSD; however, the coincidence is better than expected. The three frequencies with high PSD at the start of the disturbance (approximately at 40, 30, and 25 s) become one lower frequency at the end and are characteristic both in Figs. 10 and 11.

The main ED disturbing signal from Swarm C in Fig. 12 occurred 45 min after Mw = 7.9 EQ. It is even stronger in relation to that in Fig. 10, and the corresponding selected topside TEC disturbance is also stronger as well (see Fig. 13). Both disturbances (see Figs. 12 and 13) have more periods that are disturbed with respect to that observed in Figs. 10 and 11. The proximity of Swarm A and Swarm C may suggest that the situation has quickly evolved, and disturbances have changed rapidly. In addition, the similarity of PSD in Figs. 12 and 13 is again significant although with different geometrical references and kinds of sensors. The coincidence of PSD from LPs and GNSS TEC confirms the ionospheric origin of

the disturbances and excludes instrumental uncertainties. The observed chromatic spectra from two colocated swarm LEOs (A and C) and from two different instruments (LP and GNSS POD receiver; see Figs. 10–13), with a range of periods within [20, 40] s approximately, are in agreement with the abovementioned theory of [5].

C. Validation by Other Independent Measurements

Since the significant ionospheric disturbances from Swarm POD GNSS observation have been detected by PIES and have been confirmed by means of Swarms A and C *in situ* LP ED (Ne) measurement, it will be validated by other independent measurements for the final issue of the PIES warning.

In this work, the ground GNSS dual-frequency data will be used as the additional sources of colocated ionospheric measurements. This is due to the fact that the DORIS and other LEO POD measurements were far from the epicenter during the event. The location of the employed ground GNSS receivers is shown in Fig. 5(b). Following the processing condition used for the Swarm POD GNSS data, the same spatial window with the longitude of [140°E–167°E] and latitude of [19°S–10°N] and the time window of [10:00–12:00 UTC] are used for taking the ground GNSS data. The detrended STEC is done by the double time difference at 300 s as the bandpass filter is able to reserve most components of the acoustic-gravity wave spectra [11]. Considering the coverage of ground GNSS observations to the potential circular waves, the GNSS ionospheric combination of specific station satellites is selected for validating the PIES warning.

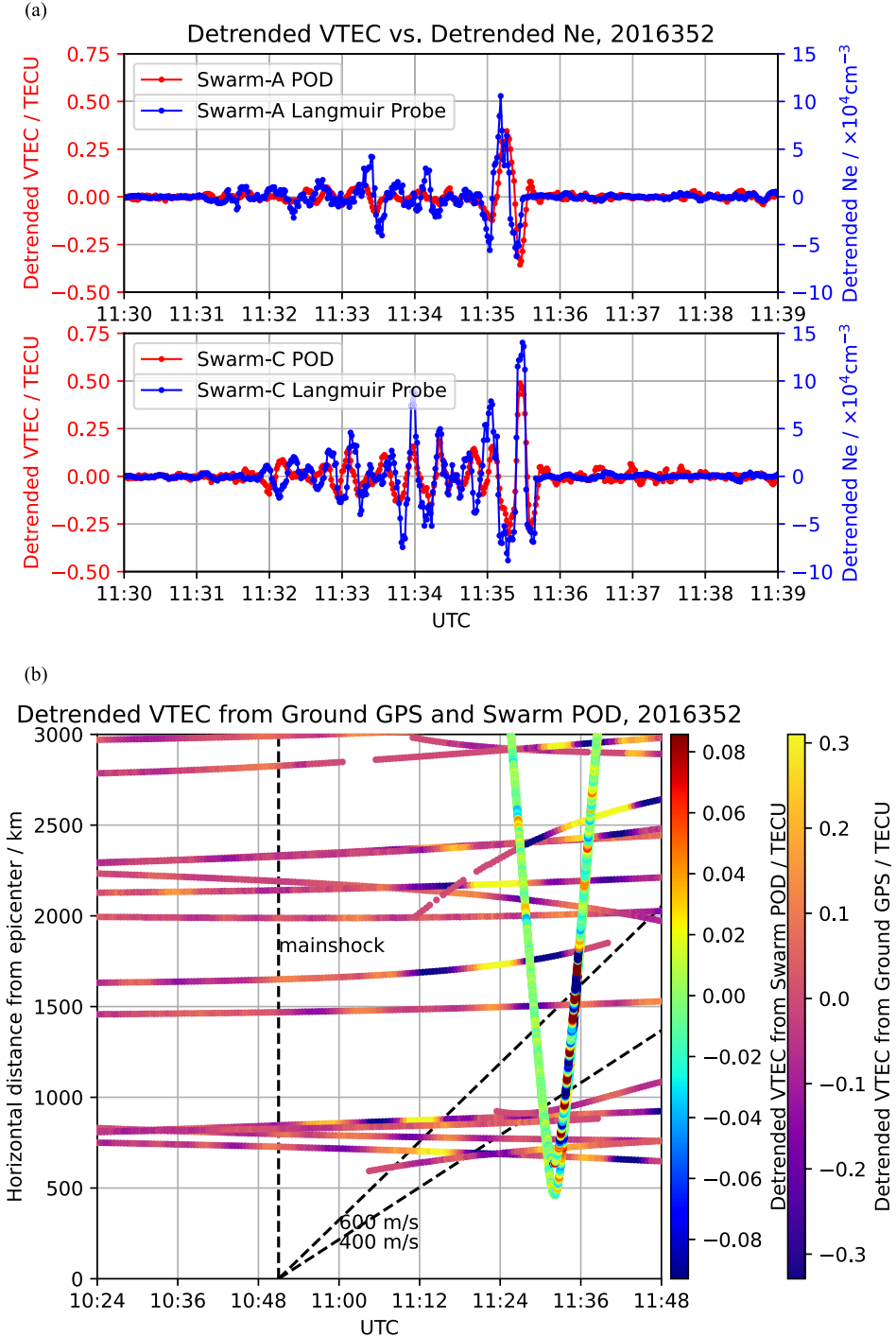


Fig. 7. (a) Evolution versus time (x -axis) of detrended GNSS POD VTEC (red) and detrended LP ED, Ne, (blue) for (Top) Swarm A and (Bottom) Swarm C during the detection of the anomalous ionospheric disturbance after the PNG Mw7.9 earthquake (10 h and 51 min of day 352, 2016). (b) Keogram of detrended VTEC from GNSS ground and POD Swarm receivers (see Fig. 5), right after PNG earthquake and coinciding with colocated Swarm pass.

As a validation, in the bottom plot of Fig. 7, the keogram of detrended VTEC measurements from the ground- and Swarm-based GNSS receivers is represented. This is done at the same time that the potential arrival times of the corresponding acoustic-gravity waves from the ground (assumed starting at E layer around 100 km, magenta dashed lines) and from the swarm LEO (cyan dashed lines, assumed at the same Swarm height (~ 460 km), supported by the almost simultaneous impact on both *in situ* ED provided by LP and in the VTEC of

POD GNSS receiver, top plot of Fig. 7), are represented. These results clearly show the compatible ionospheric response to the earthquake/tsunami at different heights.

After the mainshock, the wind field at the atmospheric pressure level of 1 hPa (at a height of around 45 km) at 11:00 UTC shows the compatible disturbing level with two normal days, i.e., days 351 and 353 of 2016 (see Fig. 14). These wind field data show no extraordinary wind conditions. Moreover, there are no extraordinary rainfall conditions during these days.

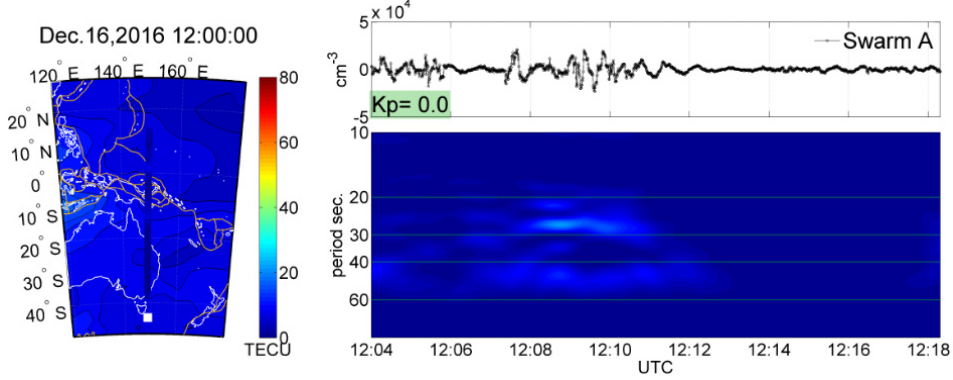


Fig. 8. Reference Swarm A high-pass filtered LP signal on December 16, 2016, at similar time of the day to disturbed signal on December 17. (Top Right) High-pass filtered LP signal (50 s) and K_p index. (Bottom Right) STFT spectrogram of the above signal. (Left) UQRG GIM with continents, tectonic plates, and Swarm LP PSD sampled at 40-s period.

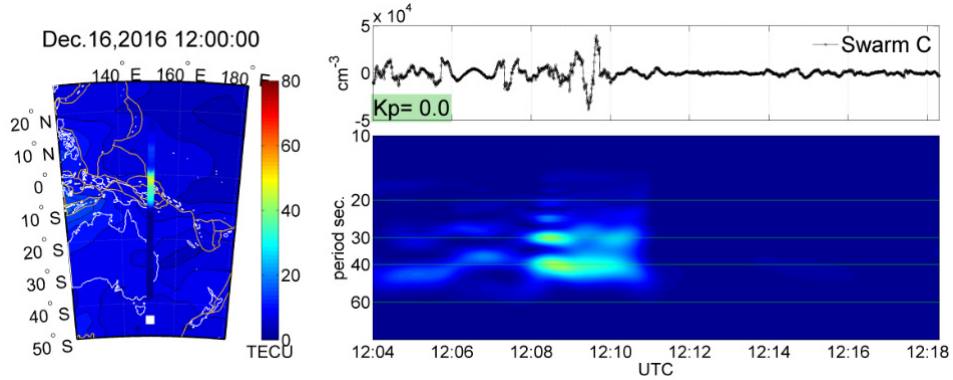


Fig. 9. Same as in Fig. 8, but for Swarm C.

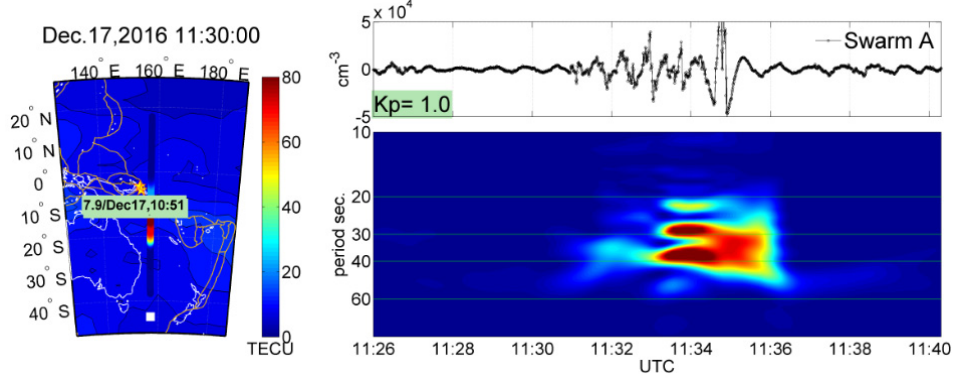


Fig. 10. Swarm A high-pass filtered LP signal on December 17, 2016, around 40 min after major EQ. (Top Right) High-pass filtered LP signal (50 s) and K_p index. (Bottom Right) STFT spectrogram of the above signal. (Left) UQRG GIM with continents, tectonic plates, and Swarm LP PSD sampled at a 40-s period. White square denotes the Swarm location in last epoch of the track.

These would indicate that meteorological conditions do not affect the AGW propagation in the middle atmosphere [62].

V. 2016 SOLOMON ISLANDS EVENT: UNEXPLAINED PRESEISMIC IONOSPHERIC SIGNATURE WITH SWARM POD

As another case study for testing PIES, we found the swarm LEO constellation approximately colocated in space and time with an earthquake and the driven tsunami occurred in the region of Solomon Islands on December 8, 2016. The tracks of Swarm satellite B recorded the topside ionospheric disturbance

regarding the 17-day background disclosed by PIES at about 1000 km west of the epicenter and about 30 min before the main earthquake shock. The magnitude of this earthquake was 7.8. For the trajectories of the corresponding ionospheric observing points (in cyan points) versus the epicenter (in red star), see Fig. 15.

A. PIES Warning Checking

Following the application of PIES to the Swarm observations in Section II, the ionospheric disturbances were extracted from the POD GPS receiver measurements and processed

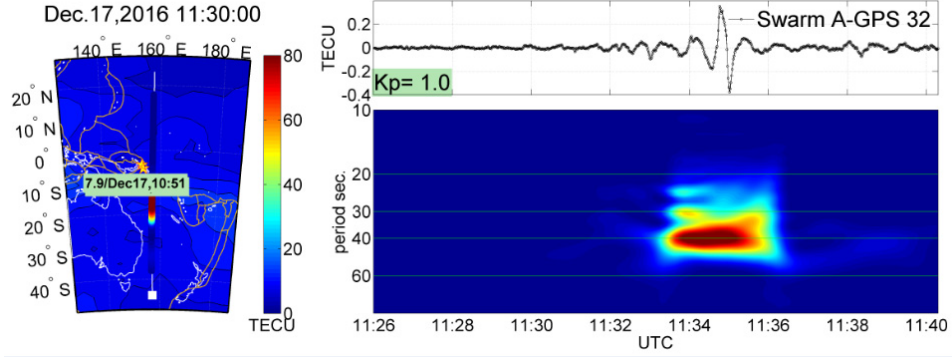


Fig. 11. Swarm A high-pass filtered topside TEC determined from Swarm A-GPS PRN 32 measurement on December 17, 2016, around 40 min after major EQ. (Top Right) High-pass filtered LP signal (50 s) and K_p index. (Bottom Right) STFT spectrogram of the above signal. (Left) UQRG GIM with continents, tectonic plates, and Swarm TEC PSD sampled at a 40-s period. The white square denotes the Swarm location in the last epoch of the track, the white line is the Swarm position with respect to colored GPS ionospheric observing points.

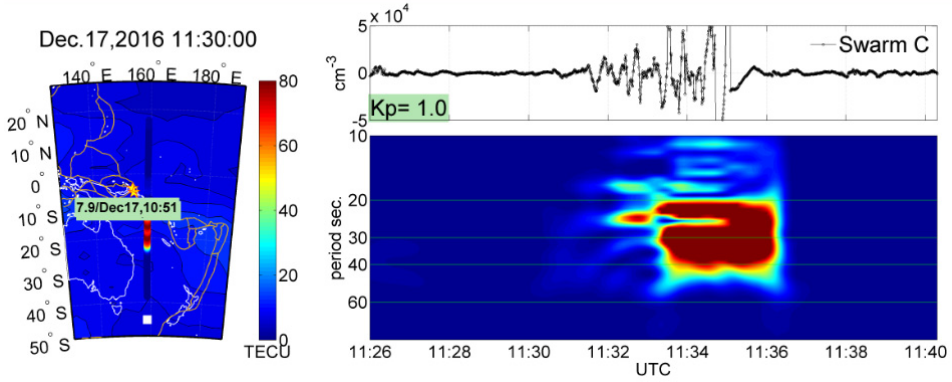


Fig. 12. Same as in Fig. 10, but for Swarm C.

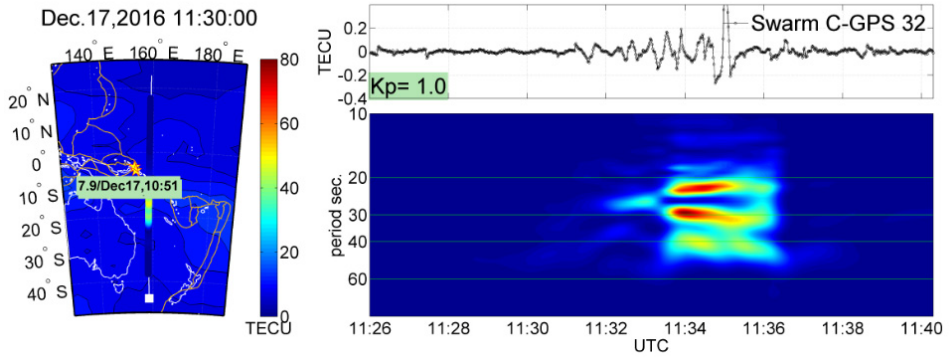


Fig. 13. Same as in Fig. 11, but for Swarm C-GPS PRN 32 pair.

with the same detrending time interval of 8 s. The detrended data showed the most significant value in the spatiotemporal window of 135°E–175°E versus 40°S–10°N versus 16:00–18:00 UTC (02:00–04:00 in the local night), so to exclude far effects of the ionosphere. The elevation mask of $\geq 40^\circ$ was taken for decreasing the potential mapping error from STEC to VTEC. The geomagnetic equatorial index $Dst = -25$ nT [58], the planetary 3-h-range index $K_p = 4$ [59], and the GOES X-ray flux measurement of Class-A [60]

indicate the moderate space weather state with no significant disturbances originated by the phenomena such as major solar activity, solar flare, or geomagnetic storm disturbances.

The detrended VTEC in Fig. 16 shows that clear ionospheric disturbances, two times the next most negative one versus the background of 17 days, occurred about 30 min before the earthquake (red versus green points), located at about one 1000 km west from the epicenter. The perturbation exhibits its maximum power at waves with a period of 16 s. As it has

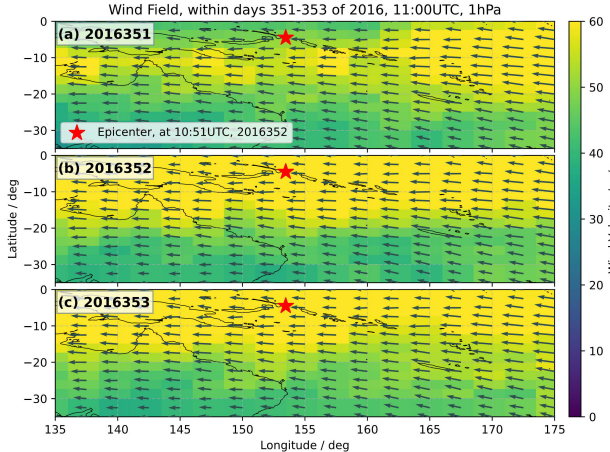


Fig. 14. Wind field at the atmospheric pressure level of 1 hPa at 11:00 UTC (a)–(c), respectively, for the days 351, 352, and 353 of 2016 [62].

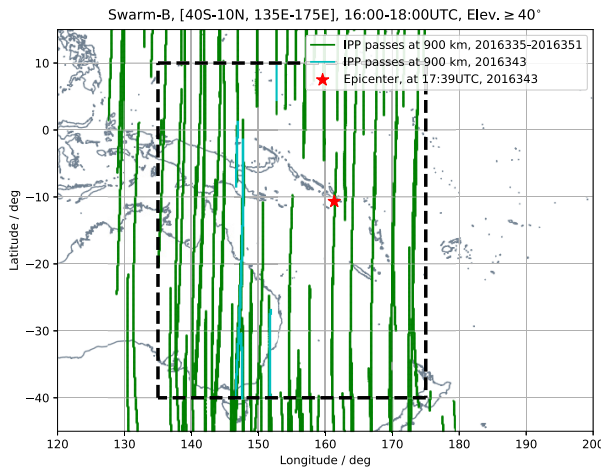


Fig. 15. Ionospheric observing points (in cyan) of Swarm B regarding GPS satellites within about 2 h before the main shock of 2016 Solomon Island earthquake, at about a 1000 km west from the epicenter, with a spatial window (135°E – 175°E versus 40°S – 10°N), with an elevation mask of 40° . The green lines correspond to the observations for 16 adjacent normal days, with the same spatiotemporal window, and elevation mask as the earthquake day, and the red star for the epicenter.

been discussed above, and taking into account the high LEO velocity and expected ionospheric wavelengths, the actual period of the perturbation should be concentrated around 12–107 s (see Section IV-A). Similar to the case study in Section IV-A, this significant disturbance [see Fig. 17(a)] was projected onto the horizontal trajectories of the ionospheric observing points regarding the corresponding Swarm satellite B [see Fig. 17(b)]. At about 17:11–17:12 UTC, the disturbances with the maximum energy locates about 1400 km southeast of the epicenter, corresponding to the detrended VTEC on the line of sight of Swarm satellite B and GPS satellite PRN 1. It is important to note that a disturbance event in the form of waves occurring before the earthquake (not necessarily an earthquake precursor) is treated in a similar way than in the previous case, i.e., as a suspicious ionospheric PIES warning, which should be further verified with different

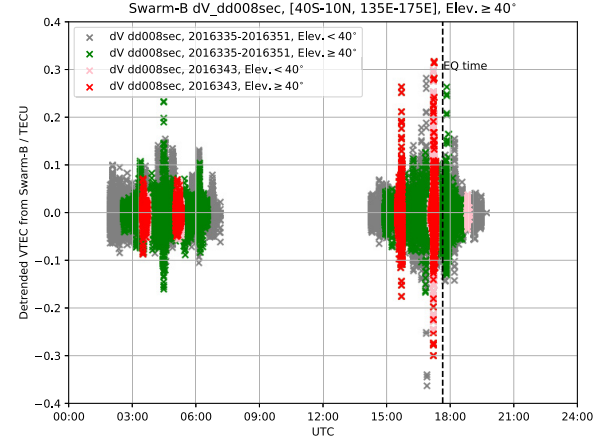


Fig. 16. Time evolution of detrended VTEC on the earthquake day (in red scatters) compared with 16 normal days with no earthquake record (in green scatters), and the gray and pink points for the detrended VTEC with the elevation of less than 40° .

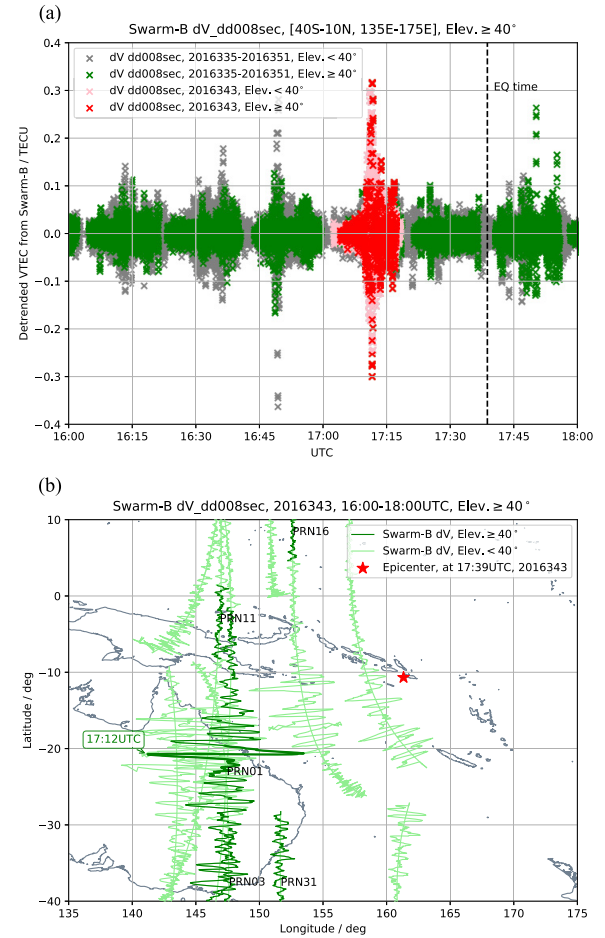


Fig. 17. (a) Zoomed time evolution of detrended VTEC during 16:00–18:00 UTC (see Fig. 16). (b) Spatial evolution of detrended VTEC horizontally overlapping ($0.1 \text{ TECU} \equiv 2^{\circ}$) the trajectories of ionospheric observing points regarding Swarm B; the plots in green or light green, respectively, for the observation with an elevation greater and lower than 40° , the bold green plots for the detected maximum disturbances, and the red star for the epicenter.

types of measurements in the following, but, regardless its interpretation, there is no consensus yet on the existence of potential earthquake ionospheric precursors; see different views in [63]–[65].

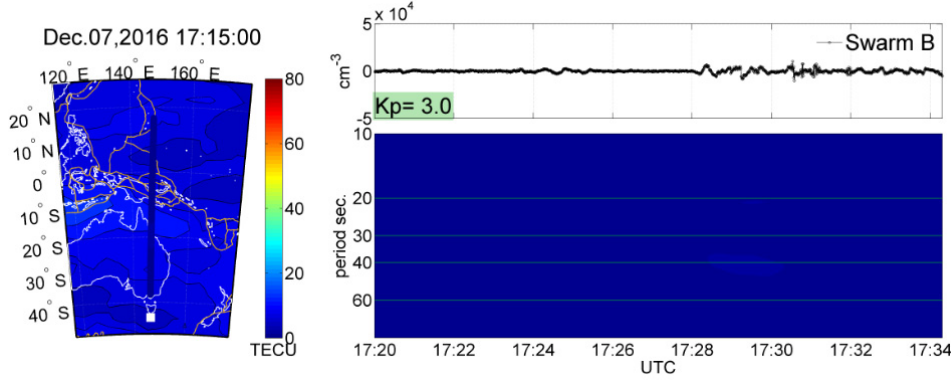


Fig. 18. Reference Swarm B high-pass filtered LP signal on December 7, 2016, at similar time of the day to disturbed signal on December 8. (Top Right) High-pass filtered LP signal (50 s) and K_p index. (Bottom Right) STFT spectrogram of the above signal. (Left) UQRG GIM with continents, tectonic plates, and Swarm LP PSD sampled at a 40-s period.

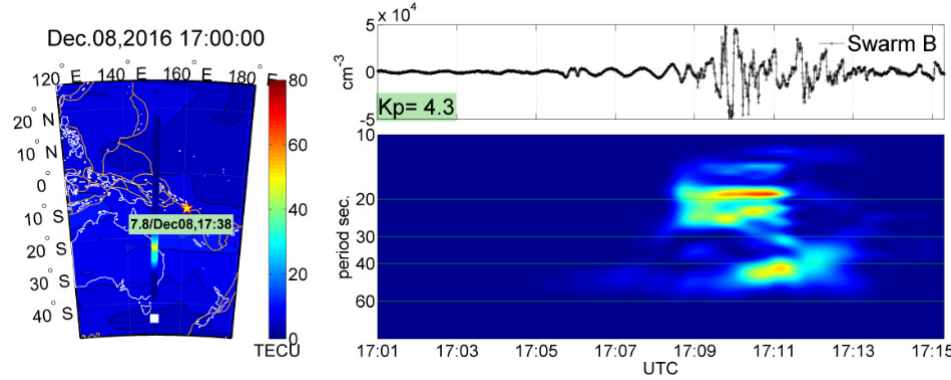


Fig. 19. Swarm B high-pass filtered LP signal on December 8, 2016, around 30 min before major EQ. (Top Right) High-pass filtered LP signal (50 s) and K_p index. (Bottom Right) STFT spectrogram of the above signal. (Left) UQRG GIM with continents, tectonic plates, and Swarm LP PSD sampled at a 40-s period.

B. Validation by Power Spectra Analysis of Swarm B Langmuir Probe ED Data

The same kind of validation with the same parameters and respective scales has been performed for Swarm B trajectories applied in PIES detection of disturbing signals at the time of $M_w = 7.8$ EQ on December 8, 2016. The selected Swarm B track was recorded on December 8, 2016, around 17:10 UTC, which is approximately 30 min before the largest $M_w 7.8$ EQ in the Solomon Islands region, occurred close to the western coast of San Cristobal island (17:38 UTC). Although the height of Swarm B is several tens of km larger than that of Swarms A and C, the high-pass filtering, the spectrograms, and their sampling have been computed using exactly the same parameters, as for Swarm A/C pair in Section IV-B. The selection of DFT filtering period thresholds in this section and Section IV-B also aims to exclude low-frequency signals from sources other than seismic or tsunami sources, e.g., geomagnetic activity increase. The correctness of this threshold in our case can be confirmed to some extent in Fig. 18, where, at the time of increasing K_p index, no disturbance can be found, at least at the magnitude level analyzed for the seismic-driven disturbances in Figs. 19 and 20. Fig. 18 uses ED data from Swarm B LPs collected on the preceding reference day of December 7, 2016. The disturbance with respect to the

common scale is almost invisible in the spectrogram in Fig. 18 (bottom right).

The situation changes markedly just before $M_w = 7.8$ EQ on December 8. Fig. 19 reveals an ED disturbance, which is somehow similar to those in Figs. 10–13, as this disturbance occupies a large number of periods/frequencies with similarly large PSD. Fig. 20 shows the corresponding selected topside TEC disturbance, where we see again some common features with the ED disturbance in Fig. 19. The disturbance starts with one common amplitude at period >40 s, with decreasing period. Then, the disturbance splits into two peaks around 30 s (which are easier to spot in the TEC plot than in the ED plot) and, later on, into two disturbances around the 20-s period, which are better recognizable in the ED signal. This coincidence confirms the ionospheric origin of the disturbance, consistent as well with the most realistic nonmonochromatic model of Vadas *et al.* [5].

C. Validation by Other Independent Measurements

Besides the confirmation by the study of Swarm B LP ED data, and due to the potential PIES warning, the validation has been complemented with two additional external sources of colocated ionospheric measurements: 1) ground GNSS dual-frequency measurements and 2) DORIS dual-frequency

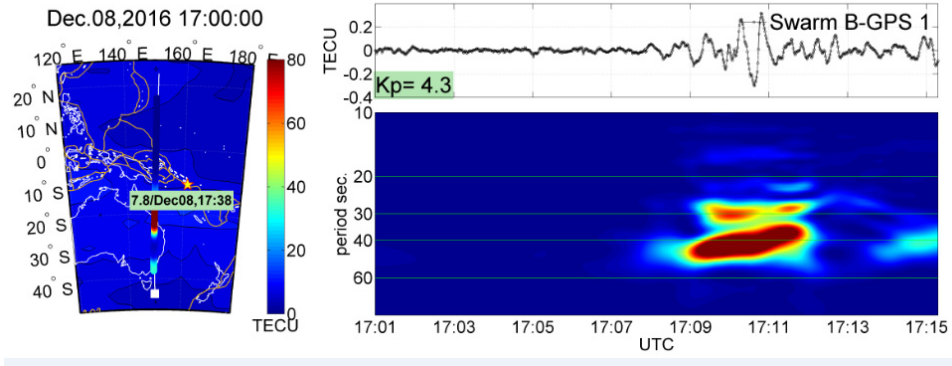


Fig. 20. Same parameters as in Fig. 19, but for topside TEC determined from Swarm B-GPS PRN 1 measurement.

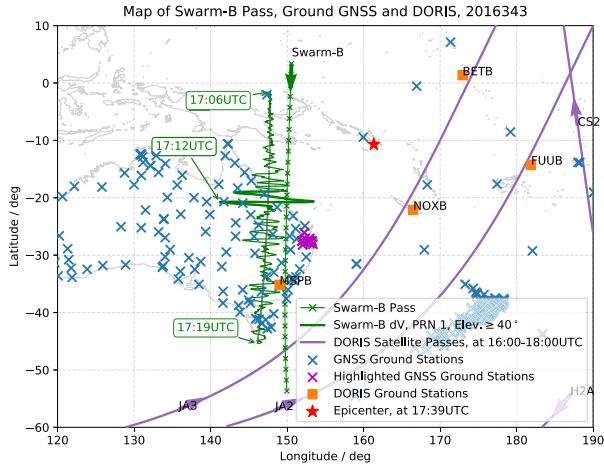


Fig. 21. Location and passes of measurements, the green line with marks for the trajectory of Swarm B, the green line for the detrended VTEC projected onto the passes of the ionospheric observing points regarding Swarm B and GPS satellite PRN 1 with greater than 40° elevation, the bold green line for the detrended VTEC with maximum energy, the purple line for passes of LEO-onboard DORIS receivers, blue marks for GNSS ground stations, magenta marks for GNSS ground stations that detected significant disturbances on the EQ day in particular, and orange rectangular for ground DORIS transmitters.

measurements. The location of the employed ground GNSS receivers, the ground DORIS transmitters, and the LEO-onboard DORIS receivers are shown in Fig. 21.

Regarding the DORIS dual-frequency measurement, the data processing has been done by the multi-TOMION model [41]. The mapping function is assumed at an effective height of 450 km regarding the disturbances, which is lower than the one assumed over the Swarm satellites for the LEO-based GPS measurements. In addition, the double difference with the time step of 20 s is used to derive the ionospheric disturbances taking into account the receiver-transmitter velocity and wavelength.

With the same processing condition used for the LEO GNSS data, i.e., the spatial window with the longitude of [135°E–175°E] and latitude of [40°S–10°N], the temporal window of the time period [16:00–18:00 UTC], the elevation mask of greater than 40°, and the detrended VTEC, including the ionospheric disturbances around the passes, of the

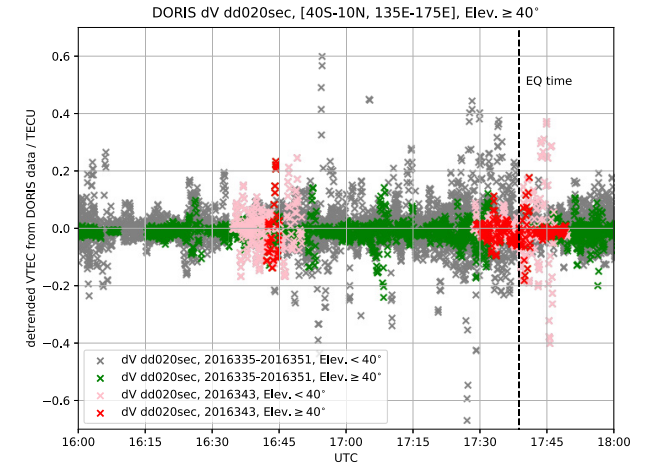


Fig. 22. Detrended VTEC of DORIS measurement during 16:00–18:00 on the earthquake day (in red), with a spatial window of [135°E–175°E] versus 40°S–10°N], compared with the adjacent days 335–351 of 2016 (in green); the observations with elevation of lower than 40° have been, respectively, marked with pink and gray.

LEO DORIS receivers on the earthquake day are shown in Fig. 22. Note that the time series showing the disturbances of increasing intensity (marked in purple in Fig. 22) at the time about 16:43–16:45 UTC (02:43–04:45 in the local night) is of interest. Following the steps of PIES, the DORIS data with the 14 neighboring days are also studied by mean of the same spatiotemporal window and the elevation mask; their time series (in green) are organized in Fig. 22, as well as the one (in red) on the earthquake day. The perturbation on detrended VTEC on the earthquake day occurred about 55 min before the earthquake, showing significantly larger intensity than the ones on the normal days, which locates at the southeast of the epicenter. In comparison to the significant disturbance measured by Swarm B, the detected disturbances might be compatible in terms of their time location (less than 30 min apart) and their latitudes although they are about 2500 km away.

The GNSS ground stations for validation were selected from the permanent GNSS networks, i.e., the Australian CORS (AUSCORS), Land Information New Zealand (LINZ), and the IGS network. Besides the TOMION model, the double time

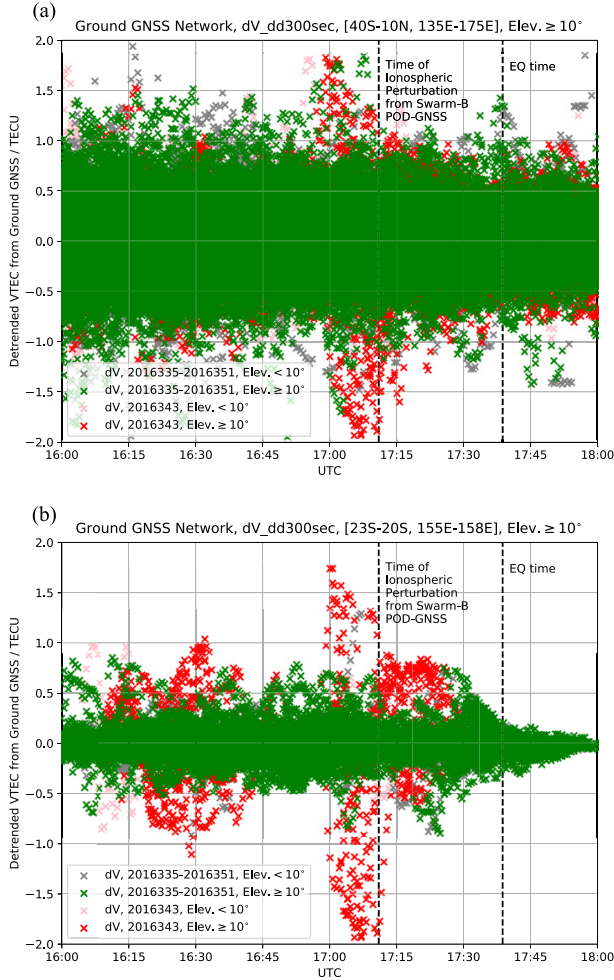


Fig. 23. (a) Detrended VTEC of Ground GNSS measurement by double difference with time step of 300 s, during 16:00–18:00 on the earthquake day (in red), with a spatial window of [135°E–175°E, 40°S–10°N], compared with the adjacent days 335–351 of 2016 (in green); the observations with elevation of lower than 10° have been, respectively, marked by pink and gray. (b) Same as (a) with a zoomed spatial window of [155°E–158°E, 23°S–20°S].

difference with two time steps at 60 and 300 s is used to find the earthquake signal in the ionosphere (see [11]) and the same spatiotemporal window than the case for Swarm satellite observation. Note that a smaller elevation mask of 10° is applied to look for the potential TIDs occurring above the ocean; see the previous case study [11]. In addition, the ionospheric effective height regarding ground GNSS is set as 250 km for studying the ionospheric disturbances lower than the F layer; see the detailed explanation in [18]. By means of the double difference with a time step of 300 s, the results of the detrended VTEC preserve a stronger intensity than that of 60 s. Since about 17:00 UTC, the results of 300 s show the most significant disturbances compared with the ones of normal days [see Fig. 23(a)]. The disturbances occurring about 3–10 min before the peak disturbance of Swarm B [see Fig. 23(b)] come from a region with the longitude of [155°E–158°E] and latitude of [23°S–20°S], which locates east of Swarm B and also southwest of the epicenter.

The original observation shown in Fig. 24(a), i.e., the GNSS ionospheric combination L_I , including such disturbances, was

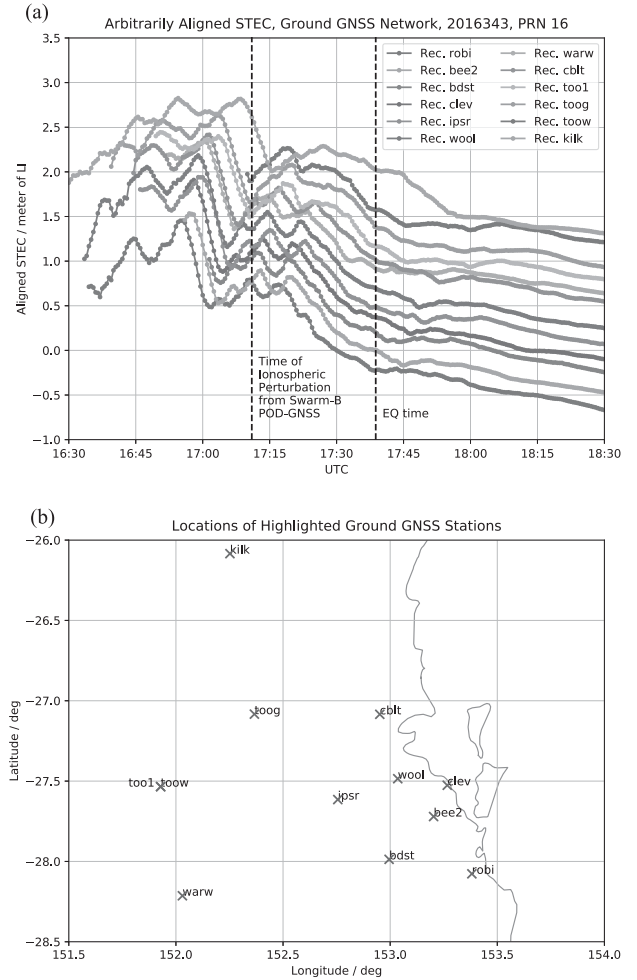


Fig. 24. (a) Time evolution of the arbitrarily aligned STECs, for the GPS satellite PRN 16, at the time of 16:30–18:50; the color codes of lines correspond to different GNSS receivers, and the black dashed line indicates the time of the earthquake at 17:39 UTC. (b) Locations regarding ground GNSS stations.

arbitrarily aligned along the time sequence of the STEC decrease. Considering the locations of GNSS receivers in Fig. 24(b), the results clearly show a group of ionospheric disturbances manifested as an “N-shape” with intensities of 2 TECUs, propagating from southeast to northwest (i.e., approximately perpendicular to the EQ epicenter direction) with a propagation velocity of about 230–270 m/s and a raw wavelength estimation of about 400–600 km. Note that the “N-shape” TEC depletion shows much slower variation than the typical ionospheric response to the large/middle magnitude earthquakes [11]. Fig. 25 shows the ionospheric disturbances derived from multiple measurements at different locations and heights. The ionospheric disturbances were detected for the first time from the DORIS observation data (i.e., the ionospheric observing points regarding the NOXB-JA2 pair, at 16:44 UTC), taken into account the estimated velocity and azimuth of propagation. The next occurrence is from ground-based GNSS measurements during 17:02–17:12 followed by measurements from Swarm B POD-GNSS. The disturbances are shown both at the topside ionosphere (by Swarm) and the lower ionosphere (by DORIS). The ionospheric disturbances

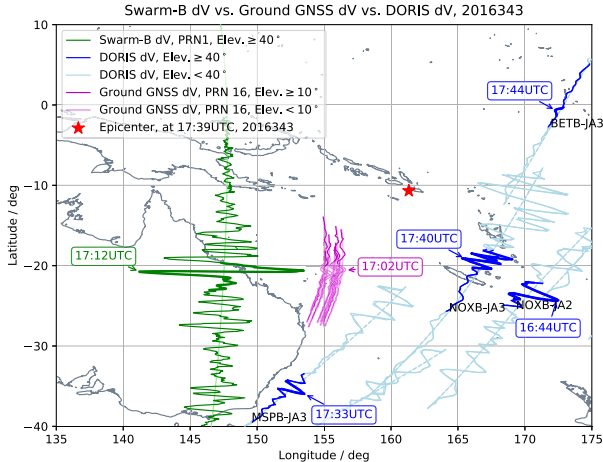


Fig. 25. Detrended VTEC comparison between results of Swarm B, Ground GNSS, and DORIS. The green line for the detrended VTEC projected onto the ionospheric observing points of GPS satellites PRN 1 from Swarm B and with the elevation mask of 40° , the blue line for the detrended VTEC projected onto the passes of the light of sights regarding ground transmitters and all LEO receivers, the purple line for the detrended VTEC projected onto the observing points regarding highlighted ground GNSS receivers and GPS satellite PRN 16, the light blue and light purple, respectively, for the ones with less than 40° and 10° , respectively, and the bold green, bold blue, and bold purple lines for the respective series of detrended VTEC with maximum energies.

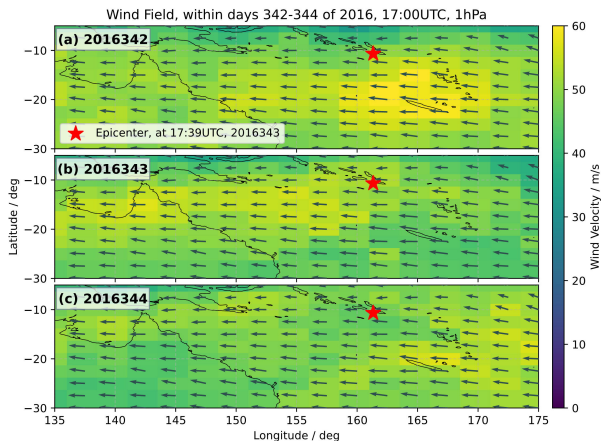


Fig. 26. Wind field at the atmospheric pressure level of 1 hPa at 17:00 UTC (a)–(c), respectively, for the days 342, 343, and 344 of 2016 [62].

appearing along the time and distance sequence are evident, as a TEC depletion and the afterward fluctuations (see Fig. 25). In summary, the results by ground stations show the consistency of the ionospheric perturbation detection in time and location with Swarm satellite B.

Finally, on the earthquake day, the wind field at the atmospheric pressure level of 1 hPa (at height of ~ 45 km) at 17:00 UTC shows the compatible disturbing level with two normal days, i.e., days 342 and 344 of 2016 (see Fig. 26), which are sourced from [62], showing no extraordinary wind conditions. Moreover, there are no extraordinary rainfall conditions during these days.

VI. CONCLUSION

We have presented the POD-GNSS LEO Detrended Ionospheric Electron Content Significant Deviations (PIES),

a method to detect the significant ionospheric disturbances from the detrended TEC of the GNSS POD LEO data, which can help in particular to identify the tsunami signatures in the topside ionosphere-based observations. The results are validated by other independent measurements. This method relying on the ongoing and historic POD GNSS measurements could be an effective tool for contributing to potential warnings of earthquakes and tsunamis based solely on LEO satellites. By analyzing POD-GNSS data from swarm LEO satellites with PIES, the topside ionospheric activities during two earthquake and tsunami cases in the PNG region in 2016 are studied. The anomalous ionospheric disturbances in the spectral ranges of tsunami-related gravity waves and earthquake-related acoustic waves are identified thanks to the collocated swarm LEO data and validated versus other sources.

The likely origin of the tsunami to explain part of the observed anomalous ionospheric signals has been determined thanks as well to a novel comparison of the required vertical velocity of the potential gravity wave associated with the tsunami. Indeed, it is consistent with the most-recent theory [5], which shows that a tsunami (which is localized in space and time) excites a spectrum of gravity waves, some of which have faster horizontal phase speeds than the tsunami. These fast gravity waves also have very high vertical phase speeds (up to 300 m/s). Our results, however, are not consistent with previous model works, which considered the tsunami as a monochromatic ocean wave (not localized in space and time). In other words, this work can be considered as a possible experimental confirmation of the most recent and realistic model of gravity wave propagation, in particular in the ionosphere.

It is also important to emphasize, in the context of the validation of PIES results, the analysis of spectral responses in LP ED signals onboard Swarm A and Swarm B and detects many ED disturbances that are coincident with persistent seismic activity in December 2016 in PNG and Solomon Islands regions. Such analysis is in good agreement with the results provided by the independent POD GNSS data. The samples of ED power spectrum at frequencies corresponding to 350–450 km along orbital arcs show the coincidence of large spectral peaks with critical seismic activity, such as first or largest earthquakes in the region, and the coincidence of low spectrum responses with the relaxation time. Similar spectral representations of disturbing signals in LP ED data are found several times, which is promising for future spectral analysis for the recognition of different disturbing signals in the ionosphere.

Regarding the PNG Mw 7.9 earthquake, the presented results can help to open a new door in the applicability of LEO POD GNSS data to contribute to the real-time LEO tsunami detection and monitoring thanks to the increasing number of GNSS LEO receivers as potential ionospheric sounders onboard of hundreds of CubeSats.

In the case of the ionospheric disturbances found before the Solomon Mw 7.8 earthquake, the highly suspicious PIES warning might enlarge the potential application of the indicator in such LEO earthquake/tsunami monitoring, which does not necessarily have to be a definite earthquake precursor warning.

Using the PIES methodology, in the passes around 30 min before the earthquake, an unexplained disturbance signal of about a 16-s period was found in the detrended VTEC (considering only elevations above 40° to minimize errors in the mapping function). This detection was done by the analysis of POD GNSS Swarm constellation data during 17 days in the region around the earthquake and tsunami held at Solomon islands. This result, unexplained so far, has been confirmed with independent LP ED, DORIS, and ground-based GNSS measurements.

The use of both ground-based data, i.e., GNSS receivers displacements near the epicenter of an earthquake, as well as the ionospheric signature of earthquakes and tsunami in their data, can provide: 1) the validation of the proposed method to also help establish the occurrence and intensity of an earthquake soon after it happens and 2) a means to develop further the technique for processing the GNSS data from artificial satellite receivers to detect in particular tsunamis from orbits higher than 450 km.

The future work can include adapting the overall PIES strategy used in PNG earthquake/tsunami and Solomon Island earthquake for real-time or nearly real-time computation and analysis.

ACKNOWLEDGMENT

The data for this article are available, and they can be requested from Heng Yang (h.yang@upc.edu) and Manuel Hernández-Pajares (manuel.hernandez@upc.edu).

REFERENCES

- [1] W. R. Peltier and C. O. Hines, "On the possible detection of tsunamis by a monitoring of the ionosphere," *J. Geophys. Res.*, vol. 81, no. 12, pp. 1995–2000, Apr. 1976.
- [2] G. Occhipinti, P. Lognonné, E. A. Kherani, and H. Hébert, "Three-dimensional waveform modeling of ionospheric signature induced by the 2004 Sumatra tsunami," *Geophys. Res. Lett.*, vol. 33, no. 20, pp. 1–5, 2006.
- [3] M. P. Hickey, G. Schubert, and R. L. Walterscheid, "Propagation of tsunami-driven gravity waves into the thermosphere and ionosphere," *J. Geophys. Res., Space Phys.*, vol. 114, no. A8, pp. 1–16, Aug. 2009.
- [4] J. J. Makela *et al.*, "Imaging and modeling the ionospheric airglow response over Hawaii to the tsunami generated by the Tohoku earthquake of 11 March 2011," *Geophys. Res. Lett.*, vol. 38, no. 24, pp. 1–5, Dec. 2011.
- [5] S. L. Vadas, J. J. Makela, M. J. Nicolls, and R. F. Milliff, "Excitation of gravity waves by ocean surface wave packets: Upward propagation and reconstruction of the thermospheric gravity wave field," *J. Geophys. Res., Space Phys.*, vol. 120, no. 11, pp. 9748–9780, Nov. 2015.
- [6] X. Meng, P. Vergados, A. Komjathy, and O. Verkhoglyadova, "Upper atmospheric responses to surface disturbances: An observational perspective," *Radio Sci.*, vol. 54, no. 11, pp. 1076–1098, Nov. 2019.
- [7] C. O. Hines, "Gravity waves in the atmosphere," *Nature*, vol. 239, pp. 73–78, Sep. 1972.
- [8] M. L. V. Pitteway and C. O. Hines, "The viscous damping of atmospheric gravity waves," *Can. J. Phys.*, vol. 41, no. 12, pp. 1935–1948, Dec. 1963.
- [9] S. L. Vadas, "Horizontal and vertical propagation and dissipation of gravity waves in the thermosphere from lower atmospheric and thermospheric sources," *J. Geophys. Res., Space Phys.*, vol. 112, no. A6, pp. 1–23, Jun. 2007.
- [10] M. Hernández-Pajares *et al.*, "The ionosphere: Effects, GPS modeling and the benefits for space geodetic techniques," *J. Geodesy*, vol. 85, no. 12, pp. 887–907, 2011.
- [11] H. Yang, E. Monte Moreno, and M. Hernández-Pajares, "ADDTID: An alternative tool for studying Earthquake/Tsunami signatures in the ionosphere. Case of the 2011 Tohoku earthquake," *Remote Sens.*, vol. 11, no. 16, p. 1894, Aug. 2019.
- [12] M. Hernández-Pajares *et al.*, "The IGS VTEC maps: A reliable source of ionospheric information since 1998," *J. Geodesy*, vol. 83, no. 3, pp. 263–275, Mar. 2009.
- [13] J. Artru, V. Ducic, H. Kanamori, P. Lognonné, and M. Murakami, "Ionospheric detection of gravity waves induced by tsunamis," *Geophys. J. Int.*, vol. 160, no. 3, pp. 840–848, 2005.
- [14] A. Komjathy *et al.*, "Detecting ionospheric TEC perturbations caused by natural hazards using a global network of GPS receivers: The Tohoku case study," *Earth, Planets Space*, vol. 64, no. 12, pp. 1287–1294, Dec. 2012.
- [15] G. Occhipinti, L. Rolland, P. Lognonné, and S. Watada, "From Sumatra 2004 to tohoku-oki 2011: The systematic GPS detection of the ionospheric signature induced by tsunamigenic earthquakes," *J. Geophys. Res., Space Phys.*, vol. 118, no. 6, pp. 3626–3636, Jun. 2013.
- [16] I. Azeem, S. L. Vadas, G. Crowley, and J. J. Makela, "Traveling ionospheric disturbances over the United States induced by gravity waves from the 2011 Tohoku tsunami and comparison with gravity wave dissipative theory," *J. Geophys. Res., Space Phys.*, vol. 122, no. 3, pp. 3430–3447, Mar. 2017.
- [17] J. Y. Liu *et al.*, "Giant ionospheric disturbances excited by the M9.3 Sumatra earthquake of 26 December 2004," *Geophys. Res. Lett.*, vol. 33, no. 2, pp. 1–3, 2006.
- [18] M. Hernández-Pajares, J. M. Juan, and J. Sanz, "Medium-scale traveling ionospheric disturbances affecting GPS measurements: Spatial and temporal analysis," *J. Geophys. Res.*, vol. 111, no. A7, pp. 1–3, 2006.
- [19] Y.-M. Yang *et al.*, "Tohoku-Oki earthquake caused major ionospheric disturbances at 450 km altitude over Alaska," *Radio Sci.*, vol. 49, no. 12, pp. 1206–1213, Dec. 2014.
- [20] A. Komjathy, Y.-M. Yang, X. Meng, O. Verkhoglyadova, A. J. Mannucci, and R. B. Langley, "Recent developments in understanding natural-hazards-generated TEC perturbations: Measurements and modeling results," in *Proc. Ionospheric Effects Symp.*, Alexandria, VA, USA, May 2015, pp. 12–14.
- [21] W. Jarmolowski, P. Wielgosz, A. Krypiak-Gregorczyk, B. Milanowska, and R. Haagmans, "Seismic ionospheric disturbances related to Chile-Illapel 2015 earthquake and tsunami observed by Swarm and ground GNSS stations," in *Proc. EGU Gen. Assembly Conf. Abstracts*. Luxembourg: Springer, Apr. 2021, pp. 19–30.
- [22] M. Schmidt, A. Goss, and E. Erdogan, "Monitoring and modelling of ionospheric disturbances by means of GRACE, GOCE and swarm *in-situ* observations," in *Proc. EGU Gen. Assembly Conf. Abstracts*. Luxembourg: Springer, Apr. 2021, pp. 19–30.
- [23] S.-C. Han, J. Sauber, and R. Riva, "Contribution of satellite gravimetry to understanding seismic source processes of the 2011 Tohoku-Oki earthquake," *Geophys. Res. Lett.*, vol. 38, no. 24, pp. 1–6, Dec. 2011.
- [24] M. J. Fuchs, J. Bouman, T. Broerse, P. Visser, and B. Vermeersen, "Observing coseismic gravity change from the Japan Tohoku-Oki 2011 earthquake with GOCE gravity gradiometry," *J. Geophys. Res., Solid Earth*, vol. 118, no. 10, pp. 5712–5721, Oct. 2013.
- [25] P. Coisson, P. Lognonné, D. Walser, and L. M. Rolland, "First tsunami gravity wave detection in ionospheric radio occultation data," *Earth Space Sci.*, vol. 2, no. 5, pp. 125–133, May 2015.
- [26] R. F. Garcia, E. Doornbos, S. Bruinsma, and H. Hebert, "Atmospheric gravity waves due to the Tohoku-Oki tsunami observed in the thermosphere by GOCE," *J. Geophys. Res., Atmos.*, vol. 119, no. 8, pp. 4498–4506, Apr. 2014.
- [27] D. A. Galvan *et al.*, "Ionospheric signatures of Tohoku-Oki tsunami of March 11, 2011: Model comparisons near the epicenter," *Radio Sci.*, vol. 47, no. 4, pp. 1–10, Aug. 2012.
- [28] M. C. Lee *et al.*, "Did tsunami-launched gravity waves trigger ionospheric turbulence over Arecibo?" *J. Geophys. Res., Space Phys.*, vol. 113, no. A1, pp. 1–12, Jan. 2008.
- [29] M. Kamogawa *et al.*, "A possible space-based tsunami early warning system using observations of the tsunami ionospheric hole," *Sci. Rep.*, vol. 6, no. 1, pp. 1–7, Dec. 2016.
- [30] A. Komjathy, Y.-M. Yang, X. Meng, O. Verkhoglyadova, A. J. Mannucci, and R. B. Langley, "Detection of natural-hazards-generated tec perturbations using ground-based and spaceborne ionospheric measurements and potential new applications," in *Proc. Ion Pacific PNT Meeting*, 2015, pp. 522–527.
- [31] A. De Santis *et al.*, "Precursory worldwide signatures of earthquake occurrences on swarm satellite data," *Sci. Rep.*, vol. 9, no. 1, pp. 1–13, Dec. 2019.
- [32] G. Olivares-Pulido, M. Hernández-Pajares, A. Aragón-Ángel, and A. García-Rigo, "A linear scale height chapman model supported by GNSS occultation measurements," *J. Geophys. Res., Space Phys.*, vol. 121, no. 8, pp. 7932–7940, Aug. 2016.

- [33] F. D. S. Prol, D. R. Themens, M. Hernández-Pajares, P. D. O. Camargo, and T. D. A. H. M. Muella, "Linear vary-chap topside electron density model with topside sounder and radio-occultation data," *Surv. Geophys.*, vol. 40, no. 2, pp. 1–17, 2019, doi: [10.1007/s10712-019-09521-3](https://doi.org/10.1007/s10712-019-09521-3).
- [34] M. Hernández-Pajares *et al.*, "Electron density extrapolation above F2 peak by the linear vary-chap model supporting new global navigation satellite systems-LEO occultation missions," *J. Geophys. Res., Space Phys.*, vol. 122, no. 8, pp. 9003–9014, 2017.
- [35] H. Lyu, M. Hernández-Pajares, E. Monte-Moreno, and E. Cardellach, "Electron density retrieval from truncated radio occultation GNSS data," *J. Geophys. Res., Space Phys.*, vol. 124, no. 6, pp. 4842–4851, Jun. 2019.
- [36] V. V. Forsythe, T. Duly, D. Hampton, and V. Nguyen, "Validation of ionospheric electron density measurements derived from spire CubeSat constellation," *Radio Sci.*, vol. 55, no. 1, Jan. 2020, Art. no. e2019RS006953.
- [37] M. J. Angling *et al.*, "Sensing the ionosphere with the spire radio occultation constellation," *J. Space Weather Space Climate*, vol. 11, p. 56, 2021.
- [38] K. Wang, A. Allahvirdi-Zadeh, A. El-Mowafy, and J. N. Gross, "A sensitivity study of POD using dual-frequency GPS for CubeSats data limitation and resources," *Remote Sens.*, vol. 12, no. 13, p. 2107, Jul. 2020.
- [39] W. Jarmolowski *et al.*, "Combining Swarm Langmuir probe observations, LEO-POD-based and ground-based GNSS receivers and ionosondes for prompt detection of ionospheric earthquake and tsunami signatures: Case study of 2015 Chile-Illapel event," *J. Space Weather Space Climate*, vol. 11, no. 58, pp. 1–28, 2021.
- [40] J. van den IJssel, J. Encarnação, E. Doornbos, and P. Visser, "Precise science orbits for the Swarm satellite constellation," *Adv. Space Res.*, vol. 56, no. 6, pp. 1042–1055, Sep. 2015.
- [41] M. Hernández-Pajares, H. Lyu, M. García-Fernandez, and R. Orús-Pérez, "A new way of improving global ionospheric maps by ionospheric tomography: Consistent combination of multi-GNSS and multi-space geodetic dual-frequency measurements gathered from vessel-, LEO- and ground-based receivers," *J. Geodesy*, vol. 94, no. 8, pp. 1–16, Aug. 2020.
- [42] N. P. Perevalova, V. A. Sankov, E. I. Astafyeva, and D. S. Zhupityaeva, "Threshold magnitude for ionospheric TEC response to earthquakes," *J. Atmos. Solar-Terrestrial Phys.*, vol. 108, pp. 77–90, Feb. 2014.
- [43] S. Jin, G. Occhipinti, and R. Jin, "GNSS ionospheric seismology: Recent observation evidences and characteristics," *Earth-Sci. Rev.*, vol. 147, pp. 54–64, Aug. 2015.
- [44] D. Marchetti, A. De Santis, S. Jin, S. A. Campuzano, G. Cianchini, and A. Piscini, "Co-seismic magnetic field perturbations detected by swarm three-satellite constellation," *Remote Sens.*, vol. 12, no. 7, p. 1166, Apr. 2020.
- [45] P. Lognonné, R. Garcia, F. Crespon, G. Occhipinti, A. Kherani, and J. Artru-Lambin, "Seismic waves in the ionosphere," *Europhys. News*, vol. 37, no. 4, pp. 11–15, Jul. 2006.
- [46] C. O. Hines, "Internal atmospheric gravity waves at ionospheric heights," *Can. J. Phys.*, vol. 38, no. 11, pp. 1441–1481, 1960.
- [47] M. Hernández-Pajares, J. M. Juan, J. Sanz, and A. Aragón-Ángel, "Propagation of medium scale traveling ionospheric disturbances at different latitudes and solar cycle conditions," *Radio Sci.*, vol. 47, no. 6, Dec. 2012.
- [48] M. Hernández-Pajares *et al.*, "Direct MSTID mitigation in precise GPS processing," *Radio Sci.*, vol. 52, no. 3, pp. 321–337, Mar. 2017.
- [49] H. Yang, E. Monte-Moreno, and M. Hernández-Pajares, "Multi-TID detection and characterization in a dense global navigation satellite system receiver network," *J. Geophys. Res., Space Phys.*, vol. 122, no. 9, pp. 9554–9575, Sep. 2017.
- [50] F. J. Harris, "On the use of windows for harmonic analysis with the discrete Fourier transform," *Proc. IEEE*, vol. 66, no. 1, pp. 51–83, Jan. 1978.
- [51] H. Yang, E. M. Moreno, and M. Hernández-Pajares, "Detection and description of the different ionospheric disturbances that appeared during the solar eclipse of 21 August 2017," *Remote Sens.*, vol. 10, no. 11, p. 1710, Oct. 2018.
- [52] A. K. Maurya, M. N. Shrivastava, and K. N. Kumar, "Ionospheric monitoring with the Chilean GPS eyeball during the south American total solar eclipse on 2nd July 2019," *Sci. Rep.*, vol. 10, no. 1, pp. 1–10, Dec. 2020.
- [53] S. L. Vadas and E. Becker, "Numerical modeling of the generation of tertiary gravity waves in the mesosphere and thermosphere during strong mountain wave events over the southern Andes," *J. Geophys. Res., Space Phys.*, vol. 124, no. 9, pp. 7687–7718, Sep. 2019.
- [54] E. Becker and S. L. Vadas, "Explicit global simulation of gravity waves in the thermosphere," *J. Geophys. Research: Space Phys.*, vol. 125, no. 10, Oct. 2020, Art. no. e2020JA028034.
- [55] J. Kong, L. Shan, X. Yan, and Y. Wang, "Analysis of ionospheric disturbance response to the heavy rain event," *Remote Sens.*, vol. 14, no. 3, p. 510, Jan. 2022.
- [56] U. Schneider, A. Becker, P. Finger, E. Rustemeier, and M. Ziese, "GPCC full data monthly product version 2020 at 1.0°: Monthly landsurface precipitation from rain-gauges built on GTS-based and historical data," Deutscher Wetterdienst (DWD), Offenbach, Germany, 2020.
- [57] X. Meng, O. P. Verkhoglyadova, A. Komjathy, G. Savastano, and A. J. Mannucci, "Physics-based modeling of earthquake-induced ionospheric disturbances," *J. Geophys. Res., Space Phys.*, vol. 123, no. 9, pp. 8021–8038, Sep. 2018.
- [58] (2016). Japan World Data Center for Geomagnetism. *Geomagnetic Equatorial Dst Data*. Accessed: Jan. 18, 2021. [Online]. Available: http://wdc.kugi.kyoto-u.ac.jp/dst_provisional/201612/index.html
- [59] (2016). Geo Forschungs Zentrum (GFZ), Potsdam. *Geomagnetic Planetary KP Data*. Accessed: Jan. 18, 2021. [Online]. Available: <http://ftp://ftp.gfz-potsdam.de/pub/home/obs/kp-ap/wdc/kp1612.wdc>
- [60] (2016). U. S. NOAA Space Weather Prediction Center (SWPC). *GOES X-ray Flux Measurement*. Accessed: Jan. 18, 2021. [Online]. Available: http://ftp://ftp.swpc.noaa.gov/pub/warehouse/2016/2016_plots/xray/20161217_xray.gif
- [61] (2016). U.S. NOAA/NWS, National Tsunami Warning Center. *Tsunami Maximum Amplitude Graph*. Accessed: Jan. 18, 2021. [Online]. Available: <https://www.tsunami.gov/previous.events>
- [62] (2019). European Centre For Medium-Range Weather Forecasts. *ERA5 Reanalysis (0.25 Degree Latitude-Longitude Grid)*. [Online]. Available: <https://rda.ucar.edu/datasets/ds633.0/>
- [63] K. Heki, "Ionospheric electron enhancement preceding the 2011 Tohoku-Oki earthquake," *Geophys. Res. Lett.*, vol. 38, no. 17, pp. 1–6, Sep. 2011.
- [64] S. Pulinets *et al.*, "Ionosphere sounding for pre-seismic anomalies identification (INSPIRE): Results of the project and perspectives for the short-term earthquake forecast," *Frontiers Earth Sci.*, vol. 9, p. 131, Apr. 2021.
- [65] R. Ikuta, T. Hisada, G. Karakama, and O. Kuwano, "Stochastic evaluation of pre-earthquake TEC enhancements," *J. Geophys. Res., Space Phys.*, vol. 125, no. 11, Nov. 2020, Art. no. e2020JA027899.



Heng Yang received the Ph.D. degree in signal theory and processing from the Universitat Politècnica de Catalunya (UPC), Barcelona, Spain, in 2019.

He is currently an Associate Professor with the School of Electronic Information and Engineering, Yangtze Normal University, Chongqing, China. He has been a Post-Doctoral Researcher with the Research Group of Ionospheric Determination and Navigation based on Satellite and Terrestrial Systems (IonSAT), Department of Mathematics, UPC. He is working on the technologies of global navigation satellite system (GNSS) ionospheric sounding, including the computation of real-time global ionospheric maps, the detection of ionospheric perturbations, and relationship with natural events.



Manuel Hernández-Pajares is currently a Full Professor and the Head of the UPC-Research Group of Ionospheric Determination and Navigation based on Satellite and Terrestrial Systems (IonSAT), Universitat Politècnica de Catalunya, Barcelona, Spain. He has been working on a global navigation satellite system (GNSS) since 1989 and on new algorithms for precise ionospheric sounding and navigation since 1994. He has been a principal investigator of more than three dozens of international scientific projects. He has published 125 articles in Q1 and Q2 peer-reviewed journals, with 7000 citations, an H-index of 39, and an i10-index of 108 (February 2022). He has coauthored six patents, most of them international.

Dr. Hernández-Pajares was the Chair of the International GNSS Service (IGS) Ionosphere WG from 2002 to 2007.



Wojciech Jarmołowski received the Ph.D. degree in physical geodesy from the Department of Geoengineering, University of Warmia and Mazury in Olsztyn, Olsztyn, Poland, in 2006.

He is currently an Assistant Professor with the Department of Geoengineering, University of Warmia and Mazury in Olsztyn. His research interests focus on geostatistical modeling of geophysical quantities [gravity and total electron content (TEC)], satellite altimetry, and low Earth orbit (LEO) mission data analysis, as well as global navigation satellite system (GNSS) geodetic and geophysical applications.



Paweł Wielgosz is currently a Full Professor with the Department of Geodesy, University of Warmia and Mazury in Olsztyn, Olsztyn, Poland, where he heads a research group on advanced methods for global navigation satellite system (GNSS) data processing. His research interests cover satellite navigation, precise positioning, and GNSS-based ionosphere and troposphere studies.

Dr. Wielgosz is also the Chair of the IAG Sub-Commission 4.4 "GNSS Integrity and Quality Control."



Sharon L. Vadas received the bachelor's degree in physics and chemistry from the University of Rochester, Rochester, NY, USA, in 1987, and the master's and Ph.D. degrees in physics from The University of Chicago, Chicago, IL, USA, in 1990 and 1993, respectively.

She is currently a Senior Research Scientist with NorthWest Research Associates, Inc., Boulder, CO, USA. Her research interest is focused on the theoretical study and modeling of atmospheric gravity waves in the Earth's atmosphere, with a special emphasis on comparison between models and data.



Oscar L. Colombo has worked on studies of space missions to map the gravity field of Earth and other bodies of the solar system on the precise determination of the orbits of artificial satellites and the modeling of forces acting on them in particular. He has also worked on several altimetric satellite missions, including ICESat 2 now in progress for mapping the ocean surface and the tides and to monitor the rise in sea level related to climate change and the corresponding changes in the volume of ice in the cryosphere, and on techniques for the precise

navigation of a variety of vehicles and precise surveying using GPS, as well as kinematic methods for the precise determination of orbits of satellites using data from GPS receivers onboard the spacecraft. He is currently a Senior Visiting Scientist with the NASA Goddard Space Flight Center, Greenbelt, MD, USA, where he is also a member of the Institute of Navigation.

Dr. Colombo is also a fellow of the International Association of Geodesy (IAG).



Enric Monte-Moreno received the bachelor's degree in telecommunication engineering and the Ph.D. degree in digital signal processing from the Universitat Politècnica de Catalunya, Barcelona, Spain, in 1987 and 1992, respectively, and the degree in philosophy and the degree in mathematics from the Universidad Nacional de Educación a Distancia, Madrid, Spain, in 2000 and 2010, respectively.

He is currently an Associate Professor with the Department of Signal Theory and Communications, Universitat Politècnica de Catalunya. His research interests include digital signal processing, automatic speech recognition, global navigation satellite system (GNSS), machine learning applied to economics, medical topics, and the study of the ionosphere.



Alberto Garcia-Rigo is currently pursuing the Ph.D. degree in aerospace science and technology and engineering of telecommunications from the Universitat Politècnica de Catalunya (UPC), Barcelona, Spain, in 2012.

He is an international expert on global navigation satellite system (GNSS)-based ionospheric determination, space weather, and positioning, with a particular focus on real-time/prediction operational systems. He is currently the Head of the Project Management Office, Institute of Space Studies of Catalonia (IEEC), Barcelona, also contributing to its Knowledge Transfer Office since September 2018.

Dr. Garcia-Rigo also chairs a Joint Working Group within the International Association of Geodesy (IAG) Global Geodetic Observing System (GGOS) Program. He has been an Associate Editor of IEEE JOURNAL OF SELECTED TOPICS IN APPLIED EARTH OBSERVATIONS AND REMOTE SENSING (JSTARS) since December 2019 and part of the Organising Committee of the ESA's 4th Symposium on Space Educational Activities (SSEA) since 2022.



Victoria Graffigna received the bachelor's degree from the Universidad Nacional de La Plata (UNLP), La Plata, Argentina, in 2015, and the master's degree from the Universitat Politècnica de Catalunya (UPC), Barcelona, Spain, in 2017. She is currently pursuing the Ph.D. degree with UNLP.

The focus of her research lies in global navigation satellite system (GNSS) processing for recovering geophysical signals.



Anna Krypiak-Gregorczyk is currently an Assistant Professor with the Institute of Geodesy and Civil Engineering, University of Warmia and Mazury in Olsztyn (UWM), Olsztyn, Poland. Her research interests cover global navigation satellite system (GNSS)-based ionosphere study.

Dr. Krypiak-Gregorczyk is also the Chair of IAG JWG 4.3.3 "Validation of VTEC models for high-precision and high-resolution applications."



Beata Milanowska received the master's degree in satellite geodesy from the Department of Geodesy, University of Warmia and Mazury in Olsztyn, Olsztyn, Poland, in 2019.

She is currently a Research Assistant with the Department of Geodesy, University of Warmia and Mazury in Olsztyn. Her research interests are ionospheric modeling and model evaluation.

Ms. Milanowska is also a member of IAG JWG 4.3.3 "Validation of VTEC models for high-precision and high-resolution applications."



Pau Bofill-Soliguer received the bachelor's degree in telecommunication engineering and the Ph.D. degree in artificial intelligence from the Universitat Politècnica de Catalunya, Barcelona, Spain, in 1986 and 1997, respectively.

His research interests are in signal separation, pattern learning, ecological economy, and engineering education.



Germán Olivares-Pulido received the bachelor's and Ph.D. degrees in physics from the Universitat Autònoma de Barcelona (UAB) in 2000 and 2007.

Since 2010, he has been working on geodetic techniques for ionospheric sounding and ionospheric modeling for global navigation satellite system (GNSS) algorithms. From 2010 to 2013, he was an Assistant Researcher with the Group of Geophysics, University of Luxembourg, Esch-sur-Alzette, Luxembourg, working on Bayesian techniques for stochastic time series analysis. In 2014, he was a Senior Researcher with the UPC-Research Group of Ionospheric Determination and Navigation based on Satellite and Terrestrial Systems (IonSAT), Universitat Politècnica de Catalunya, Barcelona, Spain, working on ionospheric modeling for satellite based augmentation system (SBAS) and first-principles ionospheric models. In 2015, he was a Senior Researcher with the University of Warmia and Mazury in Olsztyn, Olsztyn, Poland, where he helped to develop a regional ionospheric model based on Voronoi tessellation for the LOFAR project. From 2016 to April 2019, he developed a 3-D ionospheric model to support precise point positioning-real time kinematics (PPP-RTK) at the Australian Bureau of Meteorology, Melbourne, Australia. In April 2019, he joined the Space Weather Team, Spire, Glasgow, U.K., as Senior Ionosphere Modeler. Since June 2021, he has been a Senior Researcher with the UPC-IonSAT Group.



Roger Haagmans received the master's degree in geodetic engineering from the Delft University of Technology, Delft, The Netherlands, in 1988.

He continued first as a Researcher and later as an Assistant Professor of geodesy with the Delft University of Technology until 1999. In 2000, he became an Associate Professor of geodesy and surveying at the Agricultural University of Norway, Aas-NLH, Norway. In 2001, he joined the European Space Agency (ESA), Noordwijk, The Netherlands, as the Head of the Earth Surfaces and Interior Section, Earth Observation Programmes Directorate, where he is currently a Senior Advisor.



Qi Liu received the master's degree in geodesy from the University of Chinese Academy of Sciences (UCAS), Beijing, China, in 2019. He is currently pursuing the Ph.D. degree with the Universitat Politècnica de Catalunya (UPC), Barcelona, Spain.

His research interests include global navigation satellite system (GNSS)-based ionospheric sounding, space weather monitoring, and GNSS positioning.